Title

Mechanisms of Nitric Oxide Reactions Mediated by Biologically Relevant Metal Centers

Authors

Ford, Peter C
Pereira, Jose Clayston Melo
Miranda, Katrina M

Publication Date

2013

DOI

10.1007/430_2013_117

Peer reviewed

Struct Bond (2014) 154: 99–136
DOI: 10.1007/430_2013_117

Published online: 5 October 2013

Mechanisms of Nitric Oxide Reactions Mediated by Biologically Relevant Metal Centers

Peter C. Ford, Jose Clayston Melo Pereira, and Katrina M. Miranda

Abstract Here, we present an overview of mechanisms relevant to the formation and several key reactions of nitric oxide (nitrogen monoxide) complexes with biologically relevant metal centers. The focus will be largely on iron and copper complexes. We will discuss the applications of both thermal and photochemical methodologies for investigating such reactions quantitatively.

Keywords Copper · Heme models · Hemes · Iron · Metalloproteins · Nitric oxide

Contents

P.C. Ford (✉) and J.C.M. Pereira
Department of Chemistry and Biochemistry, University of California, Santa Barbara, CA 93106-9510, USA
e-mail: ford@chem.ucsb.edu

K.M. Miranda
Department of Chemistry and Biochemistry, University of Arizona, Tucson, AZ, USA
e-mail: kmiranda@email.arizona.edu

Abbreviations

AN	Acetonitrile
aq	Aqueous
Cbl	Cobalamin
cGMP	Cyclic guanylyl monophosphate
CysSH	Cysteine
Cyt^{II}	Ferrous cytochrome *c*
DAC	Bis(9-Anthracylmethyl)cyclam
DFT	Density functional theory
dmp	2,9-Dimethyl-1,10-phenanthroline
DNIC	Dinitrosyl iron complexes
dpp	2,9-Diphenyl-1,10-phenanthroline
$EDTA^{4-}$	Ethylenediamintetraacetate
EPR	Electron paramagnetic resonance
F_8Por	Tetrakis(2,6-difluorophenyl)-porphyrinato
GSH	Glutathione
GSNO	*S*-Nitrosoglutathione
GTP	Guanylyl triphosphate
Hb	Hemoglobin
Mb	Myoglobin
metMb	Metmyoglobin
MLCT	Metal-to-ligand charge transfer
MNIC	Mononitrosyl iron complexes
NiR	Nitrite reductase
NOS	Nitric oxide synthase
Por	Porphyrinato
PPIX	Protoporphyrin IX
RBS	Roussin's black salt
RRE	Roussin's red esters
RRS	Roussin's red salt
sGC	Soluble guanylyl cyclase
THF	Tetrahydrofuran
TMPS	Tetra(sulfonato-mesityl)porphyrinato
TPP	Tetraphenylporphyrinato
TPPS	Tetra(4-sulfonatophenyl)porphyrin
tren	Bis-(2-aminoethyl)amine
UV	Ultraviolet

1 Introduction

From the early studies leading to the discovery that nitric oxide (nitrogen monoxide) plays important regulatory roles in mammalian physiology, it has been clear that this bioactivity is closely connected to the interactions of NO with metal centers [1–3]. A key target is the ferroheme enzyme soluble guanylyl cyclase (sGC), which catalyzes the transformation of guanylyl triphosphate (GTP) to give the secondary messenger cyclic guanylyl monophosphate (cGMP), and the interactions of NO with this and with other metalloproteins and model compounds have been widely studied [4]. A critical feature of sGC activation is that it is triggered by very low concentrations of NO (as low as 1 nM) in aerobic media [5], and this sensitivity requires a remarkable selectivity of this enzyme for NO [6]. Furthermore, while NO may be generated by acid-catalyzed nitrite disproportionation, the principal biosynthetic pathways endogenous to mammals involve constitutive and inducible forms of the enzyme nitric oxide synthase (NOS), which are also heme proteins [7]. So, heme centers are involved both in the endogenous formation of NO and as one of the primary targets.

Thus, to understand the physiological mechanisms of NO, we need to define its direct interactions with metal centers. This includes visualizing the products formed and elucidating the dynamics and thermodynamics of these reactions. Furthermore, one needs to understand the effect of NO coordination both on the properties of the resulting metal complexes and on the reactivity of coordinated NO itself. Such effects may involve structural and reactivity changes at protein sites remote from the metal center, in analogy to the cooperative effects seen when dioxygen binds to hemoglobin. Similarly, one needs to consider the interactions of other NO_x derivatives with metals, given extensive biomedical interest in the therapeutic, signaling, and/or deleterious effects of nitroxyl (HNO), nitrite ion (NO_2^-), nitrogen dioxide, and peroxynitrite ($OONO^-$) and more complex species such as *S*-nitrosothiols (RSNO) and *N*-nitrosoamines (RR'NNO).

The goal of this article is to outline fundamental chemical processes that may be relevant to the mammalian chemical biology of NO and other key species. The focus will be on the dynamics, thermodynamics, and mechanisms of the formation and subsequent reactions of various metal-NO complexes. This will not be a comprehensive review of the huge body of work reported over the past several decades, but a selective overview of these topics.

2 Metal-Nitrosyl Bonding

NO coordinates to numerous transition metals, but we will largely focus on metal centers having biological relevance, principally iron (both heme and non-heme systems) and copper. NO typically coordinates to a metal center via the nitrogen atom, and in such M–NO complexes the character of this ligand can range from a

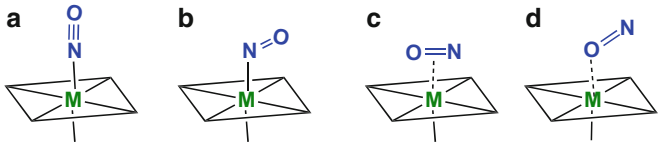

Fig. 1 Linear, bent, side-on bonding, and isonitrosyl forms of metal-NO complexes

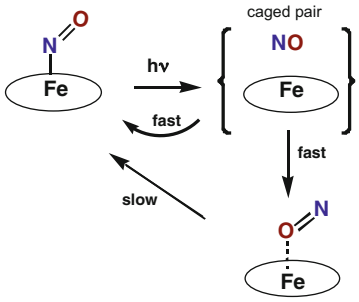

Scheme 1 Likely pathway for forming the isonitrosyl complex Fe^{II}(Por)(*O*N) by visible range photolysis of low-temperature solids (25 K KBr) containing Fe^{II}(Por)(*N*O) (*circles* represent a porphyrinato ligand, Por^{2-})

nitrosonium cation (NO^+) to a nitroxyl anion (NO^-) or somewhere in between [8]. The nitrosonium cation would be the case when considerable charge transfer from the NO to an oxidizing metal center (such as an Fe(III) heme) has occurred, leaving NO^+, which is isoelectronic to CO. Correspondingly, the M–NO^+ bond angle is roughly linear (~180°, Fig. 1a). A coordinated nitroxyl might be seen for the interaction of NO with a reducing metal, where charge transfer has occurred in the opposite direction. In that case, a more acute M–NO bond angle of ~120° (Fig. 1b) would be anticipated. Numerous metal-NO complexes fall between these extremes, as do the corresponding bond angles (see below).

There are limited examples of other types of coordination involving side-on bonding or O-coordination (Fig. 1c, d). These have largely been seen for metastable complexes generated in low-temperature solids by photochemical excitation of stable nitrosyl complex, and both types rearrange to the more stable N-coordinated form upon warming as illustrated in Scheme 1 [9, 10]. A side-on bonding mode with the NO bond perpendicular to the metal-ligand axis has also been demonstrated in the crystal structure of a copper nitrite reductase (NiR) prepared by infusing crystals of the wild-type protein with NO [11, 12]. Computational studies using density functional theory (DFT) showed the end-on Cu–NO structure to be ~40 kJ more stable than the side-on isomer for model complexes, although the difference was smaller for the protein [13, 14].

Qualitative theoretical discussions of metal-NO complexes $L_xM(NO)$, published sometime ago used Walsh orbital energy diagrams to predict the M–NO bond angles [15, 16]. The metal-nitrosyl unit was further described in terms of the

formulation $\{MNO\}^n$, where n is the sum of the metal d-electrons and the nitrosyl π* electrons [16]. Other ligands influence the structure and the nature of the M–NO bonding. For example, when there is a strong axial perturbation, as is the case with the metalloglobins, the M–N–O angle is predicted to be linear for $n \leq 6$ but bent for $n > 6$. This treatment is generally considered a good place to start discussing metal nitrosyls.

The ability to form a stable nitrosyl complex and the resulting structure of that species depend strongly on the oxidation state of the metal center. However, assigning an oxidation state to the metal of a M–NO complex is subject to considerable ambiguity, since NO is by no means an innocent ligand. It might minimize confusion to begin by treating NO as a neutral ligand and then examining the system carefully to see if it is likely that charge transfer has occurred to or from the nitrosyl ligand from or to the metal center. For example, let us compare the NO adducts $Mn^{II}(TPP)(NO)$, $Fe^{II}(TPP)(NO)$, and $Co^{II}(TPP)(NO)$ (TPP^{2-} = the tetraphenylporphyrinato dianion), which can be prepared in each case by the reaction of the $M^{II}(TPP)$ complex with free NO. These nitrosyl adducts display the respective M–N–O bond angles 176.2°, 149.2°, and 124.8° (180 K) [17]. The first is consistent with the bond angle predicted above for the $\{MnNO\}^6$ formulation as well as with assigning the charge distribution as $Mn^{I}(TPP)(NO^{+})$, since NO^{+} is isoelectronic with CO and the latter ligand generally coordinates linearly. The structure of the cobalt product would be consistent with that predicted for the $\{CoNO\}^8$ formulation or with assigning the charge distribution as a Co(III) nitroxyl complex $Co^{III}(TPP)(NO^{-})$. Notably, the M–N–O angle seen for the $Fe^{II}(TPP)(NO)$ adduct is intermediate between these extremes, and this is generally considered a ferrous complex $Fe^{II}(TPP)(NO)$. Oxidation gives the $\{FeNO\}^6$ system $Fe^{III}(TPP)(NO)$, which is isoelectronic to $Mn^{II}(TPP)(NO)$ and is predicted (and found) to be nearly linear.

The metal-N_{NO} bond lengths for the above $M^{II}(TPP)(NO)$ complexes follow the order 1.644, 1.717, and 1.837 Å for M = Mn, Fe, or Co, respectively [17]. In addition, structural studies also show that the Fe–N_{NO} bond is tilted a few degrees from perpendicular to the porphyrin plane in $Fe^{II}(TPP)(NO)$, and this is common for ferrous heme nitrosyls [18].

Non-heme iron nitrosyl complexes include the sodium salt of the nitroprusside ion $Fe(CN)_5(NO)^{2-}$, which has long been used as a vasodilator in hypertensive emergencies [19]. Chemical mechanisms potentially relevant to its bioactivity are discussed later in this review. Figure 2 illustrates some other non-heme nitrosyl complexes. Roussin's red salt (RRS) and Roussin's black salt (RBS) anions are iron/sulfur/nitrosyl clusters that have been known since the mid-nineteenth century [20, 21]. These salts and certain Roussin's red esters (RREs) have been studied as potential sources of therapeutic NO either thermally [22] or photochemically activated [23–29]. In addition, both mononitrosyl iron complexes (MNICs) and dinitrosyl iron complexes (DNICs) are drawing increasing attention with regard to their potential roles in mammalian physiology [30–34]. The structures drawn in Fig. 2 are qualitative representations of structures that have been determined using X-ray crystallography [35–38].

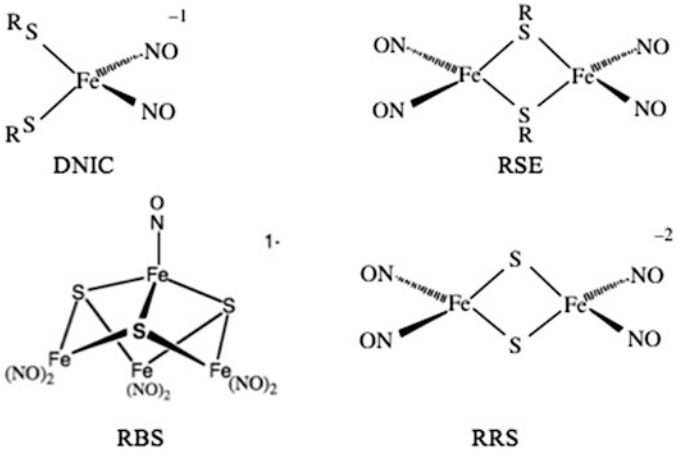

Fig. 2 Several representative non-heme iron complexes. *DNIC* dinitrosyl iron complex, *RBS* Roussin's black salt anion, *RRS* Roussin's red salt anion, *RSE* Roussin's red salt ester

Although quite a few iron complexes of NO have been isolated and characterized structurally, the list of such copper compounds is considerably shorter. In addition to the copper-NO structure described above for a NiR protein [12], the X-ray structures of a small number of model compounds have been described [13, 39, 40]. In contrast to the side-on bonded structure in the protein, the $\{CuNO\}^{11}$ complexes formed from the reaction of Cu(I) species and free NO have linear structures. Surprisingly, the structurally characterized $\{CuNO\}^{10}$ species, which is formed from the reaction of $[NO][PF_6]$ with copper in nitromethane solution, has a strongly bent structure (Cu–N–O angle of 121°) [41]. While this suggests a $Cu^{III}(NO^-)$ formulation, the NO stretching frequencies (ν_{NO} = 1,933 cm^{-1}) are much higher than expected for a nitroxyl anion, leading to the suggestion that this complex should be formulated as $Cu^{II}(NO)$. Notably, the complex is not very stable, and NO readily dissociates from the Cu coordination site.

Table 1 summarizes some structural and IR spectral data for examples of heme and non-heme iron nitrosyls and of copper nitrosyls [17, 18, 36–46].

3 How Does the Coordinated Nitrosyl Affect the Metal Center?

Electron paramagnetic resonance (EPR) spectroscopy provides insight into the electronic structure of metal nitrosyls. For example, the high-spin manganese(III) tetraphenylporphyrinato complex, Mn^{III}(TPP)(CN) ($3d^4$, $S = 2$), reacts with the free radical NO to give Mn(TPP)(CN)(NO) for which the EPR spectrum indicates an $S = 1/2$ spin state [47]. Similarly, the NO adduct of the chromium(II)

Table 1 M–NO and N–O bond lengths, M–N–O angles and IR NO stretching frequencies (ν_{NO}) for selected iron and copper nitrosyl complexes

Metal complex[a]	$\{MNO\}^{n}$ [b]	M–NO (Å)[c]	N–O (Å)[c]	Fe–N–O angle (°)[c]	ν_{NO} (cm^{-1})	References
Heme models and proteins						
Fe^{II}(TPP)(NO)	$\{FeNO\}^{7}$	1.717	1.122	149.2	1,670	[42]
Fe^{II}(T_{piv}PP)(NO)	$\{FeNO\}^{7}$	1.716	1.197	143.8	1,665	[43]
Fe^{II}(TPP)(NO)(MeIm)	$\{FeNO\}^{7}$	1.743	1.121	142.1	1,625	[44]
hh-Mb(NO)	$\{FeNO\}^{7}$	1.87	1.20	144		[18]
		2.13	1.17	120		
sw-Mb(NO)	$\{FeNO\}^{7}$	1.87	1.15	112		[46]
T-state-h-Hb(NO)						
α-heme	$\{FeNO\}^{7}$	1.74	1.13	150		[47]
β-heme		1.75	1.15			
$[Fe^{III}(OEP)(NO)]^{+}$	$\{FeNO\}^{6}$	1.644	1.112	176.9	1,868	[17]
$[Fe^{III}(TPP)(H_2O)(NO)]^{+}$	$\{FeNO\}^{6}$	1.652	1.150	174.4	1,937	[17]
$[Fe^{III}(OEP)(NO)(MeIm)]^{+}$	$\{FeNO\}^{6}$	1.647	1.135	177.3	1,921	[17]
Non-heme iron complexes						
$Na_2[Fe(CN)_5(NO)]$	$\{FeNO\}^{6}$	1.63	1.13	178.3	1,945	[35]
$Fe_2[(\mu\text{-}SC_2H_5)_2(NO)_4]$	$\{Fe(NO)_2\}^{9}$	1.675 (ave.)	1.171 (ave.)	168.5 (ave.)	1,774 s, 1,749 s, 1,819 w	[36]
$[N(PPh_3)_2][Fe(NO)_2I_2]$	$\{Fe(NO)_2\}^{9}$	1.68	1.145 (ave.)	166 (ave.)	1,775 1,719	[37]
Copper complexes						
Cu(TpRR')(NO)	$\{CuNO\}^{11}$	1.759	1.108	163.4	1,712	[42]
Cu(L3')(NO)	$\{CuNO\}^{11}$	1.786	1.035	176.4	1,742	[43]
$[Cu(NM)_5(NO)][PF_6]_2$	$\{CuNO\}^{10}$	1.955	1.109	121.0	1,933	[41]

[a]*TpRR'* tris(3-R,5-R'-pyrazolyl)hydroborate, *L3'* HC(3-tBu-5-iPrpz)$_3$, *4-Me-pip* 4-methyl-piperidine, *MeIm* 1-methyl imidazole, *NM* nitromethane. See Sect. 6 for other abbreviations

[b]Feltham/Enemark parameter *n* for the notation $\{MNO\}^{n}$, where *n* is the total number of d-electrons from the metal and π* electrons from NO [16]

[c]As determined by X-ray crystallography

porphyrin Cr^{II}(TPP) ($3d^4$, $S = 2$) exhibits an EPR spectrum consistent with an $S = 1/2$ spin state, while the reaction of NO with Mn^{II}(TPP) or Fe^{III}(Por) ($S = 5/2$) gives adducts with $S = 0$ [47, 48]. Thus, NO coordination usually gives strong field, low-spin complexes with such metal centers.

Similarly, the high-spin-state $3d^6$ ferrous analogs Fe^{II}(Por) ($S = 2$) coordinate NO to give low-spin ($S = 1/2$) Fe^{II}(Por)(NO) complexes. The EPR spectra of these complexes show super hyperfine splitting due to the nitrogen atom of the axial NO, indicating the unpaired electron density to be largely in the d_{z^2} orbital of the iron [47]. The spectra display three unique *g* values consistent with the non-axial symmetry and the bent form of the Fe–N=O moiety, in accordance with the X-ray structure (Table 1). Nitrosyl adducts of ferroheme proteins with a histidine residue in the *trans* (proximal) axial site display N hyperfine splitting of both NO and the histidine imidazole [49].

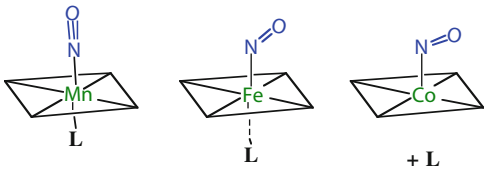

Fig. 3 Illustrated is the effect of electronic configuration on the bonding between NO and a divalent metal tetraphenylporphyrinato complex and the effect of NO coordination on the proximal ligand. Mn(II) gives a $\{MnNO\}^6$ species with a linear Mn–NO bond angle and a stable 6-coordinate complex. Fe(II) gives a $\{FeNO\}^7$ species with a bent Fe–NO bond angle and a weaker and more labile proximal ligand. Co(II) gives a $\{CoNO\}^8$ species that has a more acute M–NO bond angle and is five-coordinate. In all cases, coordination of NO switches the high spin M^{II}(TPP) complexes from high spin to low spin

The optical spectra of metalloporphyrins are dominated by characteristic π–π* porphyrin ligand bands in the near UV and visible regions [50]. The spectral shifts induced by NO coordination can be diagnostic, especially in solution studies [47, 51].

For a six-coordinate $L_5M(NO)$ complex, the model described above for $\{MNO\}^n$ complexes also predicts that going from $n = 6$ to $n = 7$ will weaken the proximal M–L bond *trans* to the NO owing to the axial σ-antibonding nature of the iron d_{z^2} orbital where much of the added electron density localizes [16]. This effect is demonstrated by structural studies of the porphyrin complex M^{II}(TPP)(L)(NO) (L = 4-methylpiperidine) [52]. For $M = Mn^{II}$ ($n = 6$), not only is the Mn–NO angle nearly linear (176°); the Mn–N_{pip} bond length is relatively short (2.20 Å). For $M = Fe^{II}$ ($n = 7$), the Fe–NO angle is bent to 142°, and the bond to the methylpiperidine is considerably weakened (Fe–N_{pip} = 2.46 Å). For $M = Co^{II}$ ($n = 8$), the Co–NO angle is even sharper, and a stable complex with methylpiperidine could not be isolated. As we will see below, such a perturbation, which is illustrated in Fig. 3, can have a profound impact on the activity of metalloproteins.

It was on the basis of this *trans* labilizing effect for the $n = 7$ case that Traylor and Sharma proposed a mechanism for sGC activation by NO [53]. Soluble guanylyl cyclase is a heme enzyme with a Fe^{II}(PPIX) ("hemin," PPIX = protoporphyrin IX) as the metal center with an open axial coordination site (the distal site). The *trans*, or proximal site, is occupied by a histidine nitrogen. Coordination of NO to the heme center gives the $\{FeNO\}^7$ complex, and the associated *trans*-influence on the metal-ligand bonding weakens the proximal histidine-iron bond. The result is a change in the protein conformation that activates the enzyme by several orders of magnitude. This model follows an earlier discussion of the electronic origins of the NO induced *trans*-effect in Fe^{II} nitrosyl complexes introduced by Mingos in 1973 [16]. It also follows the application of this concept by Perutz and coworkers [54] to explain different quaternary structural changes induced by the addition of inositol hexaphosphate to the O_2, CO, and NO adducts of hemoglobin.

An impressive test of the Traylor/Sharma model for sGC activation by NO was offered by Burstyn and coworkers [55], who investigated the activities of non-native sGC prepared by substituting Mn^{II}(PPIX) and Co^{II}(PPIX) for the hemin of the native enzyme. Addition of NO failed to activate sGC(Mn) above basal activity, presumably because the proximal histidine was not labilized in this $\{MnNO\}^6$ complex. In contrast, NO addition to sGC(Co) giving a $\{CoNO\}^8$ complex resulted in even greater activity than with sGC that had been reconstituted with hemin. The overall trend sGC(Co)(NO) > sGC(Fe)(NO) >> sGC(Mn)(NO) substantiates the Traylor/Sharma hypothesis [53] that the *trans*-effect of NO on proximal ligand lability is responsible for the activation of wt-sGC by NO. (It should be noted, however, that subsequent studies of sGC activation have proposed additional subtleties, including possible involvement of a second NO [56].)

The effect of NO coordination on the ligands *trans* to the M–NO bond has also been addressed computationally for several $\{MNO\}^6$ and $\{MNO\}^7$ systems [57–62]. For the latter complexes the interaction between the axial d_{z^2} orbital of the metal and the half-filled π* orbital of the bent nitrosyl ligand leads to weakening of the bond to the ligand *trans* to the nitrosyl as suggested by the Traylor/Sharma hypothesis. Correspondingly, a strongly bonding proximal ligand can weaken the M–NO bond in heme nitrosyl complexes, and this property may play an important role in labilizing NO from the ferroheme center in certain complexes (see below).

4 The Formation and Decay of Metal Nitrosyls

4.1 Some General Considerations

In this section we will be concerned with the reaction of a metal center with NO to form a metal-nitrosyl complex ((1), L and X are other ligands) as well as the reverse, the dissociation, or displacement of a coordinated NO (2). Although M–NO species can be formed by various pathways including the reduction of nitrite ion, the direct reaction is especially relevant to potential roles of the free NO generated by nitric oxide synthase in tissue or various biological fluids. Thus, it is necessary to have a sound understanding of the rate laws and dynamics of such reactions and of the mechanisms by which they proceed. The reverse reaction is equally of interest, given that this step may be a key determinant in the formation of NO from NOS among various biological roles. In general, the mechanisms for the forward and back reactions will occur along analogous reaction coordinate(s) as dictated by the "principle of microscopic reversibility." Much of our focus here will be on reactions involving either heme iron or non-heme iron.

$$ML_nX + NO \xrightarrow{k_{on}} ML_n(NO) + X, \quad (1)$$

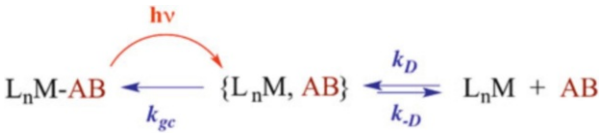

Scheme 2 Formation of a geminate pair of a diatomic molecule AB and the metal complex L_nM prepared either by flash photolysis of the AB complex or by diffusion of AB to L_nM

$$ML_n(NO) + Y \xrightarrow{k_{off}} ML_nY + NO. \quad (2)$$

Since NO is a free radical, a key question is whether its ligand substitutions on metal centers occur by mechanisms analogous to those of other small ligands such as CO that are not free radicals. Various studies have shown a substitution reactivity pattern for NO similar to that seen for other Lewis bases; however, there clearly are differences. Since the odd electron of NO resides in the π^* orbital, it very likely does not become involved in the overall bonding until the metal-NO bond is largely formed, so in this regard, a key question might be whether the transition state lies early or late along the reaction coordinate.

One example where the reactivity difference between NO and CO is quite apparent concerns the back reaction of the geminate pairs {L_nM, AB} formed by flash photolysis[1] of a L_nM-AB complex (Scheme 2, AB = NO, CO, or similar small molecule). An analogous encounter pair would also be expected to form by the diffusion of L_nM and AB together. For cases where L_nM is incorporated into a protein, such as the heme centers in myoglobin (Mb) or hemoglobin, ultrafast laser flash photolysis has been used to probe the dynamics of such geminate pairs. Typically the kinetics display significant differences between NO and CO, the recombination of the metal center with NO being much faster. In this context, Fig. 4 illustrates the different $\Delta G^{\ddagger}$ barriers for geminate recombination of ferrous Mb with NO, O_2, and CO [63]. The barrier for the recombination with NO is so small that very little NO escapes from the protein pocket upon flash photolysis of the Mb(NO) adduct owing to efficient recombination. In contrast, the barrier is much larger for the recombination with CO, so the quantum yields for photo-induced release of CO from Mb(CO) are much greater. These differences have been attributed in part to the required spin-state changes undertaken by the Mb upon coordination of these ligands [64, 65]. Interpreting these kinetics data required proposing a distribution of geminate pair configurations and protein conformations, each characterized by its own recombination rate [66, 67]. A similar behavior has been noted for other heme proteins [68].

[1] The flash photolysis kinetics studies generally employ a pump-probe approach. Typically, the pump pulse is delivered from a laser. The time frame of the experiment will depend in part upon the length of the laser pulse, which in some systems can be as short as a few fs. The probe can be a continuous or pulsed source at wavelengths ranging from the ultraviolet into the infrared depending upon the detection system, the time constant of which is typically matched to that of the pump system.

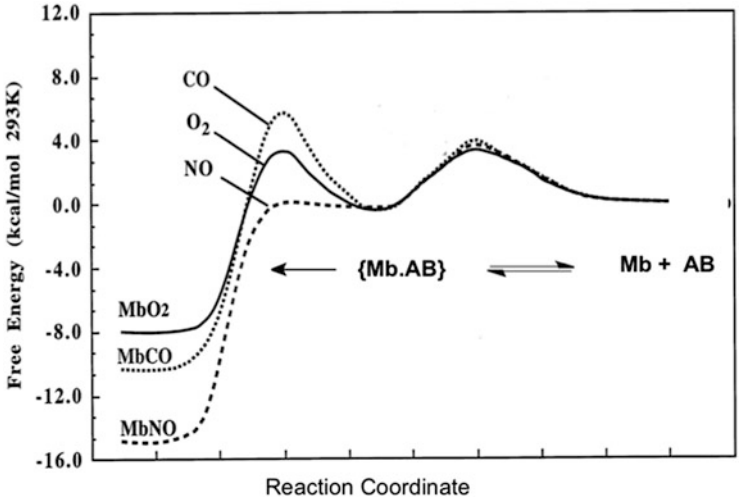

Fig. 4 Illustration of the different barriers defining the kinetics of the geminate recombination of Mb with CO, O_2, or NO (adapted from [63])

Another example where ligand free radical character apparently plays a role is the slow reaction of NO with the d^5 ruthenium(III) complex ion $Ru(NH_3)_6^{3+}$ (3). Taube and coworkers [69] studied the aqueous solution kinetics of this process and found the second-order rate constant to be much larger ($k_{NO} = 0.2\ M^{-1}\ s^{-1}$ at 298 K) than the replacement of NH_3 by typical Lewis bases such as water. As a result these workers concluded that the reaction proceeds by an associative pathway, whereby the paramagnetic Ru(III) center engages the NO radical to give a seven-coordinate intermediate $[Ru(NH_3)_6(NO)]^{3+}$, which then loses NH_3. This mechanism gains further support from subsequent studies of the temperature [70] and hydrostatic pressure effects [71] on the kinetics that determined the activation enthalpy $\Delta H^{\ddagger}$ to be small (36 kJ mol^{-1}), the activation entropy $\Delta S^{\ddagger}$ to be large and negative (–138 J K^{-1} mol^{-1}), and the activation volume $\Delta V^{\ddagger}$ also to be large and negative ($-13.6\ cm^{-3}\ mol^{-1}$).

$$Ru(NH_3)_6^{3+} + NO + H^+ \longrightarrow Ru(NH_3)_5(NO)^{3+} + NH_4^+. \quad (3)$$

Interestingly, Armor and Pell [70] found entirely different products when the reaction of $Ru(NH_3)_6^{3+}$ with NO was carried out in alkaline solution. Above pH 8.3, the sole ruthenium product was the Ru(II) dinitrogen complex $Ru(NH_3)_5(N_2)^{2+}$. Under these conditions the dominant reaction is not ligand substitution but instead appears to be NO attack on a coordinated amide ligand ($-NH_2^-$) coupled with reduction of the ruthenium [72]. Although this is an unusual mechanism, we will see below that a similar pathway can be invoked to describe the reactivity of certain copper(II) complexes used as NO sensors.

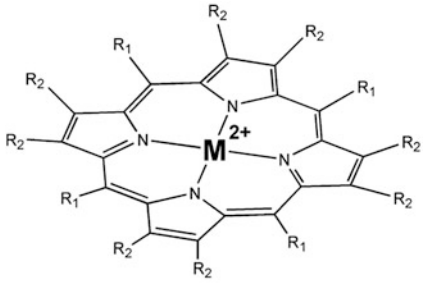

Scheme 3 Illustration of some M(Por) complexes are discussed here. TPP has R_1 = Ph and R_2 = H. TPPS is the same except that the phenyl groups are sulfonated to provide water solubility, and OEP has R_1 = H and R_2 = Et. Porphinato, which is often used in computational modeling, has R_1 = H and R_2 = H

4.2 Rates of NO Reactions with Hemes and Heme Models

Given their importance to the chemical biology of NO, it is not surprising that the formation and decay of nitrosyl complexes of heme proteins and of ferrous and ferric porphyrins heme models (Scheme 3) have been subject to considerable scrutiny. The very strong UV/visible absorptions of the metalloporphyrins and the sensitivity of these bands to the nature of the axial ligands make these systems ideal for using optical spectroscopy to follow the reaction dynamics with experimental time constants ranging from hours to less than a picosecond. The biological relevance of the "on" and "off" reactions (4) is emphasized by noting that the activation of sGC involves such an "on" reaction where the acceptor site of sGC is a Fe^{II}(PPIX) moiety. Nitric oxide effects such as cytochrome oxidase inhibition also involve coordination at heme iron, so delineating the "on" reaction dynamics is crucial to understanding NO biochemistry. Similarly, processes such as sGC deactivation and NO generation by NOS must involve Fe–NO bond labilization, so the "off" reaction dynamics are equally important.

$$\mathrm{M(Por)} + \mathrm{NO} \underset{k_{\mathrm{off}}}{\overset{k_{\mathrm{on}}}{\rightleftharpoons}} \mathrm{M(Por)(NO)}. \tag{4}$$

Early flash photolysis studies of nitrosyl heme protein and heme model complexes [73–77] actually preceded recognition of NO's importance as a bioregulator. For example, flash lamp photolysis techniques were used to determine quantum yields (Φ_{dis})[2] for CO, O_2, and NO release from the respective myoglobin complexes as ~1.0, $<10^{-2}$ and $<10^{-3}$, while photo-induced NO loss from the ferric

[2] The quantum yield Φ is a quantitative measure of the photoreaction efficiency and can be defined as the number of moles of the photoproduct formed (either transiently or permanently) per Einstein of light *absorbed* by the system.

metmyoglobin analog metMb(NO) gave a Φ_{dis} of ~1.0 [75]. Subsequent studies using faster ns laser flash photolysis techniques [76] reported a Φ_{dis} of 0.1 for NO loss from the ferrous model heme complex Fe^{II}(PPIX)(1-MeIm)(NO), much larger than for Mb(NO) but still significantly less than unity. The larger Φ_{dis} for Fe^{II}(PPIX)(1-MeIm)(NO) relative to Mb(NO) was interpreted in terms of a mechanism in which NO photolabilization first gives a {heme:NO} "encounter pair" surrounded by a solvent cage or embedded in a protein pocket as illustrated above in Scheme 2. Separation of this geminate pair was presumed to be much more facile for the solvated heme model than from the protein pocket. The result is that the NO undergoes recombination with the metal in the latter case more readily than it does diffusion away to give net ligand labilization. This scheme has been confirmed by a number of ultrafast flash photolysis studies that observed the geminate pair directly and have probed the influence of protein structure (as modified by site-directed mutagenesis) on the efficiency and dynamics of the ligand escape relative to recapture [63, 66, 68, 78, 79].

$$\mathrm{Mb(AB)} \xrightarrow{h\nu} \mathrm{Mb} + \mathrm{AB}. \tag{5}$$

The much higher net photolability of nitrosyl metalloporphyrins in the absence of the protein was further demonstrated by ns laser flash photolysis (355 nm) studies of the ferrous complexes Fe^{II}(TPP)(NO) in benzene solution [80] and Fe^{II}(TPPS)(NO) (TPPS = tetra(4-sulfonatophenyl)porphyrin) in aqueous solution [81]. In these cases, Φ_{dis} values for NO photolabilization were 0.5 and 0.16, respectively. However, for such measurements, the measured value Φ_{dis} may be dependent upon the time interval of observation. If the back reaction to re-form the original complex is facile (6), products initially formed by the photochemical step may have low steady-state concentrations; thus, the apparent Φ_{dis} values measured under low-intensity continuous photolysis would be small. However, the products would be directly observable using flash photolysis techniques with the appropriate time resolution.

$$\mathrm{M(Por)(NO)} \underset{k_{on}[\mathrm{NO}]}{\overset{h\nu}{\rightleftharpoons}} \mathrm{M(Por)} + \mathrm{NO} \tag{6}$$

NO photodissociation from nitrosyl metalloporphyrins is commonly reversible, so pulsed laser techniques are well suited for investigating the kinetics of the nitrosylation reaction. In such studies, flash photoexcitation using a pulsed laser is used to labilize NO from the M(Por)(NO) precursor, and subsequent relaxation of the non-steady-state system back to equilibrium (4) is monitored spectroscopically, usually in the presence of excess NO (Fig. 5) [82]. Under these conditions, the transient spectra would decay exponentially to give the observed rate constant k_{obs} for the return of the system to equilibrium. For the simple model photoreaction indicated by (4), a plot of k_{obs} vs. NO concentration should be linear according to (7), where the slope k_{on} equals the rate constant for the second-order thermal back

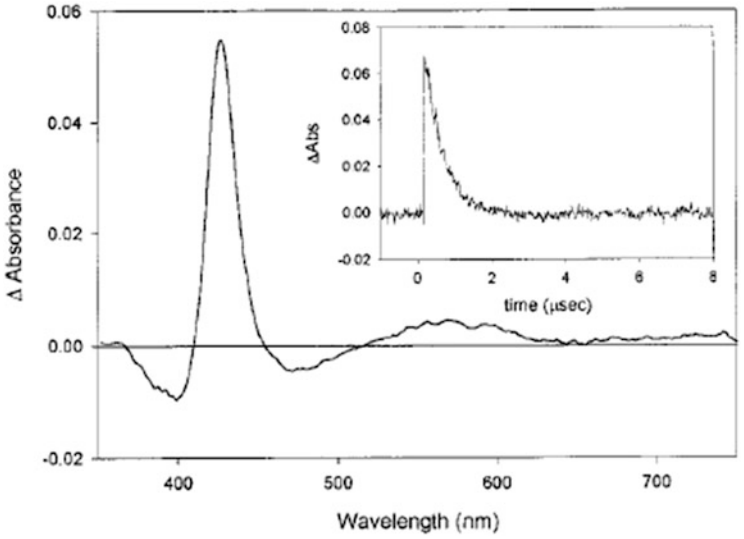

Fig. 5 Transient difference spectrum 50 ns after 355 nm flash photolysis of Fe^{II}(TMPS)(NO). *Inset*: Relaxation to equilibrium at 426 nm (Adapted with permission from [82]. Copyright 2001 American Chemical Society)

reaction and the intercept k_{off} is the overall rate constant for spontaneous (thermal) NO release from the complex.

$$k_{obs} = k_{on}[NO] + k_{off} \tag{7}$$

The equilibrium constant K_{NO} for the formation of M(Por)(NO) from M(Por) and NO under those conditions can be calculated from the ratio k_{on}/k_{off}. For example, k_{on} and k_{off} values have been determined using the flash photolysis kinetics technique for the nitrosyl complexes of metMb, ferri cytochrome *c* and catalase, and the K_{NO}'s so measured agreed well with values measured by static spectroscopic methods. However, when K_{NO} is very large, this is not a reliable method for measuring k_{off}, since the intercept in that case is often of the same magnitude as the experimental error. This is a common problem with ferrous heme protein and model nitrosyls, since they typically display very high K_{NO} values and very small k_{off} values. To address this, k_{off} can be sometimes determined by following the thermal disappearance of the M(Por)(NO) by trapping any NO released by using another compound with a very high affinity for NO, therefore serving as a NO sink. One trapping agent that has proved useful in this regard is the Ru(III) complex Ru(EDTA) [83]. However, this method is only accurate if the spontaneous NO release rate is not perturbed by the presence of the trapping agent.

Time-resolved spectroscopy has been used to define the kinetics of numerous nitrosyl metalloproteins and models under ambient conditions. Table 2 provides some examples of rate constants measured for various ferrous and ferric heme

Table 2 Representative k_{on} and k_{off} (298 K) values for Fe(II) and Fe(III) heme models and proteins in near neutral aqueous solutions unless noted (Adapted from Table 1 of [84], Copyright: American Chemical Society)

	k_{on} (M^{-1} s^{-1})	k_{off} (s^{-1})	Reference
Fe^{III} models/proteins[a]			
Fe^{III}(TPPS)[b]	4.5×10^5	500	[82]
Fe^{III}(TMPS)[c]	9.6×10^5	51	[82]
Fe^{III} (TMPS)(OH)[d]	7.4×10^3	1.5	[85]
metMb[e]	1.9×10^5	13.6	[81]
metMb[f]	4.8×10^4	43	[83]
Cyt^{III} [g]	7.2×10^2	4.4×10^{-2}	[81]
Cat [h]	3.0×10^7	1.7×10^2	[82]
	1.3×10^7	1.6	[79]
eNOS [i]	8.2×10^5	70	[86]
nNOS [j]	2.1×10^7	40	[87]
NPn [k]	$1.5–5.5 \times 10^6$	0.006–12.7	[88]
P450 CYP125 [l]	17.1×10^6	11.2	[89]
$P450_{cam}$ CYP101[m]	0.32×10^6 (34.5×10^6)	0.35 (1.93)	[90]
Fe^{II} models/proteins			
Fe^{II}(TPPS)[b]	1.5×10^9	6.4×10^{-4}	[82]
$Hb_4{}^T$ [n]	2.6×10^7	3.0×10^{-3}	[63]
$Hb_4{}^R$ [n]	2.6×10^7	1.5×10^{-4}	[63]
sGC [o]	1.4×10^8	6-8 $\times 10^{-4}$	[91]
sGC [p]	–	5.0×10^{-2}	[91]
Mb [q]	1.7×10^7	1.2×10^{-4}	[63]
Cyt^{II} [r]	8.3	2.9×10^{-5}	[81]
eNOS [s]	1.1×10^6	70	[86]
nNOS [t]	1.1×10^7	~0	[87]
P450 BM3 [u]	4.7×10^6	13.8	[92]
P. aeruginosa cd_1 NiR^v	3.9×10^8	~27.5, 3.8	[93]

[a]*eNOS* endothelial nitric oxide synthase, *nNOS* neuronal nitric oxide synthase, *NPn* nitrophorin
[b]298 K, pH 3
[c]282 K, pH 3
[d]283 K, pH 11
[e]298 K, sperm whale skeletal metMb
[f]298 K, horse heart metMb
[g]293 K
[h]293 K
[i]283 K, 1 mM arginine
[j]pH 7.8, 293 K, heme domain
[k]Range of 298 K rate constants for NPn1, NPn2, NPn3, and NPn4, pH 5.0 and pH 8.0; the k_{off} displays two phases
[l]10°C
[m]25°C, pH 7.4; values in parentheses are rate constants for camphor-bound protein
[n]293 K; two phases are observed for NO binding
[o]pH 7.4, 293 K, 3 mM Mg^{2+}, 0.5 mM GTP
[p]Phosphate buffer pH 7.0, 293 K
[q]H_2O, pH 6.5
[r]283 K, 1 mM arginine
[s]pH 7.8, 293 K, heme domain
[t]pH 7.0, 283 K
[u]30°C, pH 7.0
[v]20°C, pH 7

proteins and models [63, 81–93] and illustrates the range of k_{on} and k_{off} values found for ferriheme and ferroheme proteins. As noted above, the small values of k_{off} for the latter lead to very large K_{NO}'s, although ferrous cytochrome *c* (Cyt^{II}) is an exception. The latter also displays a very small k_{on}, presumably owing to the six-coordinate nature of Cyt^{II} for which the axial sites are occupied by an imidazole nitrogen and a methionine sulfur of the protein, so that forming a nitrosyl complex requires both ligand displacement and protein conformational changes. There are other ferrous heme proteins such as neuroglobin and the nonsymbiotic hemoglobin from *Arabidopsis thaliana* (AHb1) that exist in equilibrium between a six-coordinate form with histidines occupying both axial sites and a five-coordinate form [94, 95]. Understandably, the six-coordinate form is considerably less reactive with NO than is the five-coordinate analog. The ferric forms of catalase and nNOS are both more reactive than the model complex Fe^{III}(TPPS). Thus, it appears that in these cases, the protein structure accelerates nitrosyl formation; in contrast, the k_{off} values for metMb, Cyt^{III}, and cat are all smaller than for Fe^{III}(TPPS), consistent with retardation of NO dissociation by those proteins.

The usually small k_{off} values for the ferroheme proteins are relevant to the question of how soluble guanylyl cyclase, once activated by forming an NO complex, is turned off. Stopped-flow kinetics techniques were used by Koesling and coworkers to study loss of NO from sGC-NO [91], and these workers reported a first-order rate constant of ~7×10^{-4} s^{-1} in 293 K, pH 7.4 buffered solution. This is a k_{off} value typical of ferroheme globins (Table 2). When excess substrate guanylyl triphosphate (GTP, 5 mM) and the cofactor Mg^{2+} (3 mM) were present, the rate was significantly faster ($k_{off} \sim 5 \times 10^{-2}$ s^{-1}), and a subsequent study suggested that the in vivo rate of sGC deactivation may be several orders of magnitude higher [96].

Although ferrous nitrosyl porphyrinato complexes and ferrous nitrosyl heme proteins are commonly assumed to be unreactive toward NO dissociation, it is clear from the k_{off} values listed in Table 2 that there is a wide range of NO dissociation rates. Several of the proteins listed are as much as five orders of magnitude more reactive than Mb(NO), for example, a notable feature being that the more labile species have thiolates as proximal ligands. In this context, computational studies on the simple system Fe^{II}(P)(L)(NO) (where P^{2-} is the dianion of porphine) have shown that the Fe–NO bond length is predicted to be longer (and weaker) when the proximal ligand L is a thiol or thiolate than when L is H_2O or an imidazole [59, 61]. While it is not surprising that the proximal ligand may have a major effect on the lability of a ferroheme coordinated NO, this topic remains to be explored systematically.

4.3 Mechanistic Studies of NO "On" and "Off" Reactions with Hemes and Heme Models

While it is clear from the experiments cited above that formation of nitrosyl heme complexes are generally much faster if the distal and proximal coordination sites are not both occupied by a strongly bonding ligand, this observation does not define whether the mechanism of NO attachment is associative or dissociative. To address this issue, Laverman and coworkers [82, 83] used laser flash photolysis kinetics to probe temperature and hydrostatic pressure effects on the rates of NO reactions with the water-soluble complexes Fe^{III}(Por) (Por = TPPS or TMPS) and for metMb. In each case, the iron(III) centers are six-coordinate, but unlike the ruthenium(III) example discussed above, the axial H_2O ligands are quite labile. These kinetics data were then used to calculate the enthalpies, entropies, and volumes of activation ($\Delta H^{\ddagger}$, $\Delta S^{\ddagger}$ and $\Delta V^{\ddagger}$) for the "on" and "off" reactions. The large and positive activation entropies and volumes for both k_{on} and k_{off} are strong indications of substitutions dominated by ligand dissociation ((8) and (9)).

$$Fe^{III}(Por)(H_2O)_2 \underset{k_{-1}}{\overset{k_1}{\rightleftharpoons}} Fe^{III}(Por)(H_2O) + H_2O, \tag{8}$$

$$Fe^{III}(Por)(H_2O) + NO \underset{k_{-2}}{\overset{k_2}{\rightleftharpoons}} Fe^{III}(Por)(H_2O)(NO). \tag{9}$$

This mechanism implies that H_2O exchange with $Fe^{III}(Por)(H_2O)_2$ should be much faster than the reaction with NO, and this was indeed previously been reported by Hunt et al. for $Fe^{III}(TPPS)(H_2O)_2$ ($k_{ex} = 1.4 \times 10^7\ s^{-1}$ in 298 K water) [97]. Furthermore, these workers reported $\Delta H^{\ddagger}_{ex}$ (57 kJ mol^{-1}) and $\Delta S^{\ddagger}_{ex}$ (+84 J K^{-1} mol^{-1}) values similar to the respective k_{on} activation parameters for the NO reaction with $Fe^{III}(TPPS)(H_2O)_2$ (69 kJ mol^{-1} and 95 J K^{-1} mol^{-1}). A subsequent study by van Eldik et al. using NMR techniques [98] reported $\Delta H^{\ddagger}_{ex} = 67$ kJ mol^{-1}, $\Delta S^{\ddagger}_{ex} = +99$ J mol^{-1} K^{-1}, and $\Delta V^{\ddagger}_{ex} = +7.9$ cm^3 mol^{-1} for $Fe^{III}(TPPS)(H_2O)_2$ in even better agreement with the k_{on} activation parameters for the reaction of NO with this heme model ($\Delta V^{\ddagger}_{on} = 9 \pm 1$ cm^3 mol^{-1}) [82]. Thus, the solvent exchange kinetics for $Fe^{III}(TPPS)(H_2O)_2$ confirm that the k_{on} activation parameters are largely defined by ligand dissociation, the limiting step being (8). Notably, the k_{on} activation parameters for metMb are similar ($\Delta H^{\ddagger}_{on} = 63$ kJ mol^{-1}) with large and positive values of $\Delta S^{\ddagger}_{on}$ (+55 J mol^{-1} K^{-1}) and $\Delta V^{\ddagger}_{on}$ (+20 ± 6 cm^3 mol^{-1}), so the protein apparently does not change the mechanism [83].

Coordination of NO to the high-spin iron of Fe^{III}(Por) is accompanied by considerable charge transfer to give a linearly bonded, diamagnetic complex that can be formally represented as $Fe^{II}(Por)(NO^+)$. Thus, the activation parameters for k_{off} should also reflect the intrinsic entropy and volume changes associated with the spin change and solvent reorganization as the charge relocalizes on the metal.

This argument is consistent with the large and positive $\Delta V^{\ddagger}_{off}$ values for Fe^{III}(Por)(H_2O)(NO) ($\Delta V^{\ddagger}_{off}$ = +18 and +17 cm^{-3} mol^{-1} for Por = TPPS and TMPS, respectively) [82]. The principle of microscopic reversibility tells us that the lowest-energy pathway of the "off" reaction should involve the same reactive intermediates as the "on" reaction ((8) and (9)).

Laverman also investigated the flash photolysis kinetics of the water-soluble ferrous complexes Fe^{II}(TPPS) and Fe^{II}(TMPS) in the presence of excess NO [82]. As is common for ferrous heme globins and models, the "on" rates are ~3 orders of magnitude faster than for the ferric analogs (Table 2). Correspondingly, the activation parameters for k_{on} are consistent with processes largely defined by diffusion, even though the rate constants are about an order of magnitude less than diffusion limits in water. Since the ferroheme center may be five-coordinate in such cases, formation of the metal-NO bond would not be rate-limited by ligand labilization, but instead would reflect the formation of an encounter complex such as illustrated in Scheme 2.

The "off" reactions for ferrous models such as Fe^{II}(TPPS)(NO) are too slow to measure by the flash photolysis technique. When trapping methods were used in an attempt to evaluate loss of NO from Fe^{II}(TPPS)(NO), k_{off} values were found to be quite small but were sensitive to the nature of the trapping agents used, since Lewis bases that could coordinate at the proximal site appeared to accelerate NO loss [82]. More reliable estimates for the uncatalyzed "off" reaction were obtained by using $Ru(EDTA)^{-}$ as a NO scavenger, and the k_{off} values listed for Fe^{II}(TPPS)(NO) in Table 2 was obtained in this manner.

4.4 Non-Heme Iron Complexes

Given the growing interest in the biological chemistry of the nitrosyl complexes of non-heme iron, especially the DNICs [31–34, 99–103], there is a need to have a better understanding of the rates and mechanisms of the reactions leading to the formation and decay of such species. It has been shown that dinitrosyl iron species (DNICs) are rapidly formed in cells from the chelatable iron pool (CIP) by the reaction with NO donors [32]. Notably, such reactions have not been studied as extensively or quantitatively as those of the metalloporphyrin complexes, although some information is available through a combination of techniques.

For example, when a neutral aqueous solution of Roussin's red salt anion $Fe_2(\mu\text{-}S)_2(NO)_4^{2-}$ (RRS^{2-}, Na^+ salt) was subjected to flash photolysis, the spectral changes and kinetics behavior indicate one NO is labilized to give the $Fe_2(\mu\text{-}S)_2(NO)_3^{2-}$ anion (10) [104]. The back reaction is quite fast with a second-order rate constant of $k_{on} = 9.1 \times 10^8\ M^{-1}\ s^{-1}$. In aerated solution, this intermediate is competitively trapped by the more plentiful O_2 ($k_{ox} = 5.6 \times 10^7\ M^{-1}\ s^{-1}$) to give (eventually) the stable Roussin's black salt anion $Fe_4S_3(NO)_7^-$ (RBS^-). In a separate study by Samina et al. [105], the rates of spontaneous NO release from several dinuclear DNICs including RRS (11) were investigated by following

changes in the optical spectrum of hemoglobin, which traps the NO as it is released to give Hb(NO). For RRS^{2-}, the first-order rate constant k_{off} measured in this way was 0.061×10^{-3} s^{-1}. Accordingly, we can estimate the equilibrium constant for NO dissociation from RRS^{2-} (11) from the ratio k_{off}/k_{on} as $K_{11} = \sim 10^{-13}$ M.

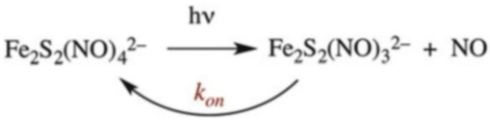

(10)

$$Fe_2S_2(NO)_4^{2-} \rightleftharpoons Fe_2S_2(NO)_3^{2-} + NO. \quad (11)$$

Analogous flash photolysis studies were carried out on the anionic Roussin's red ester $Fe_2(\mu\text{-}SCH_2CH_2SO_3)_2(NO)_4^{2-}$ in aqueous solution. These gave a k_{on} value of 1.1×10^9 M^{-1} s^{-1} for the reaction equivalent to that described by (10) [26]. Although k_{on} has not been measured for this compound, it has been determined for several similar esters, and k_{off} values of (1–9) $\times 10^{-3}$ s^{-1} were found [105]. Thus, the equilibrium constant for NO dissociation from such RSEs would appear to be about 10^{-12} M.

Flash photolysis studies of Roussin's black salt anion $Fe_4S_3(NO)_7^-$ displayed similar reversible NO photodissociation in aqueous solutions [106]. In this case, two back reaction pathways with k_{on} values of 1.3×10^7 and 7.0×10^5 M^{-1} s^{-1} were observed. A time-resolved optical and infrared spectroscopic study revealed two separate intermediates, both of which react with NO to re-form the parent complex. The identities of the intermediates are interpreted in terms of photolytic loss of chemically distinct nitrosyls found on the $Fe_4S_3(NO)_7^-$ anion. The "off" reaction rates have not been reported, but must be slow.

Despite reports that dinitrosyl-iron complexes are the most abundant nitric oxide-derived cellular adducts [34], quantitative investigations of DNIC formation are quite limited. Vanin and coworkers [107] studied the reaction between Fe^{2+}, nitrosothiol (RSNO), and thiol (RSH = cysteine or glutathione) and demonstrated that first a mononitrosyl iron complex $Fe(NO)(RS)_n$ is formed followed by formation of the DNIC $[Fe(NO)_2(RS)_2]^n$ ((12) and (13)). MNIC formation apparently occurs by a direct reaction between *S*-nitrosothiols and Fe^{2+} ions with rate constants of 3.0 and 30 M^{-1} s^{-1} for *S*-nitrosoglutathione and *S*-nitrosocysteine, respectively (100 mM Hepes buffer, pH 7.4). Since deoxyhemoglobin does not inhibit subsequent formation of DNIC, the reaction apparently does not require the release of free NO from the RSNO.

$$\left[\mathrm{Fe^{II}(RS^-)}_x\right]^{(2-x)+} + \mathrm{RSNO} \rightarrow \left[\mathrm{Fe(NO)(RS^-)}_x\right]^{(2-x)+} + \mathrm{RS}, \quad (12)$$

$$\left[\mathrm{Fe(NO)(RS)}_x\right]^{(2-x)+} + \mathrm{RSNO} \rightarrow \left[\mathrm{Fe(NO)_2(RS)_2}\right]^{+} + (x-1)\ \mathrm{RS^-}. \quad (13)$$

The reaction of NO with the simple aqueous complex $Fe(H_2O)_6^{2+}$ may be an important first step in the formation of DNICs from iron in the chelatable iron pool, and the kinetics of this reaction has been studied by Wanat et al. using stopped-flow and flash photolysis kinetics techniques [108]. The k_{on} and k_{off} values determined were, respectively, $1.42 \times 10^6\ M^{-1}\ s^{-1}$ and $3.2 \times 10^3\ s^{-1}$ (25°C). On the basis of the activation parameters, it was argued that this reaction follows an interchange dissociative mechanism, similar to that for the water exchange reaction with $Fe(H_2O)_6^{2+}$. Given that the DNICs are very stable toward NO dissociation, the relatively small equilibrium constant for (14) ($K_{12} = k_{on}/k_{off} \sim 4 \times 10^2\ M^{-1}$) is noteworthy.

$$\mathrm{Fe(H_2O)_6}^{2+} + \mathrm{NO} \underset{k_{off}}{\overset{k_{on}}{\rightleftharpoons}} \mathrm{Fe(H_2O)_5(NO)}^{2+}. \quad (14)$$

Schneppensieper et al. [109] have determined the rates and activation parameters for NO reactions with different ferrous aminocarboxylato complexes in aqueous solution. The k_{on} values ranged from 10^5 to $10^8\ M^{-1}\ s^{-1}$ ($2.4 \times 10^8\ M^{-1}\ s^{-1}$ for Fe^{II}(EDTA)), while k_{off} values were in the range 4 to $91\ s^{-1}$ ($91\ s^{-1}$ for Fe^{II}(EDTA)). The reaction of NO with Fe^{II}(EDTA) gave a $\Delta V^{\ddagger}_{on}$ of +4.1 $cm^{-3}\ mol^{-1}$, and a dissociative interchange mechanism was proposed.

4.5 Other Metal Centers of Biological Interest

The mammalian chemical biology of NO includes interactions with Cu centers. However, although a limited number of copper(I) and copper(II) nitrosyl complexes have been prepared, there have been few kinetics studies probing the formation and dissociation of such species. The ligand substitution reactions of both Cu(II) and Cu(I) are generally very fast owing to the high lability of their coordination spheres. So, in this context, one might expect the NO "on" reactions to be similarly fast. However, given that Cu–NO complexes tend to be unstable, the "off" reactions are also likely to be relatively fast. One study of Cu–NO ligand substitution reactions involved the flash photolysis of a model system consisting of a heme model complex and a second copper complex in solution (at varying ratios) under an inert atmosphere as a model for heme–copper oxidases [110]. The two components were the six-coordinate ferrous species, $Fe^{II}(F_8Por)(NO)(THF)$ [F_8Por = tetrakis (2,6-difluorophenyl)porphyrinate^{2-}), while the other was a $Cu^{I}L$ unit (L = the tridentate ligand bis-(2-pyridylmethyl)(benzyl)amine or the tetradentate ligand tris(2-pyridylmethyl)-amine). Flash photolysis led to NO labilization from

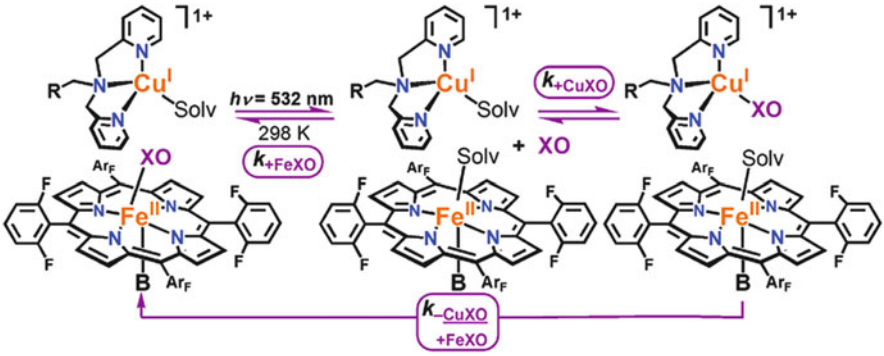

Scheme 4 Illustration showing the flash photolysis of a mixture of a Cu^{I} complex (R = phenyl or 2-pyridyl) with a NO or CO (XO) complex of $Fe^{II}(F_8Por)$ (B = THF when XO = NO) in THF solution. Photolysis-induced XO labilization is followed by trapping by the Cu^{I}, followed by slower transfer of XO back to the Fe^{II} center (Reprinted with permission from [110]. Copyright 2009 American Chemical Society)

$Fe^{II}(F_8Por)(NO)(THF)$ followed by competitive NO trapping by the Fe^{II} and Cu^{I} centers. Subsequently, a slower, first-order process was observed, indicating that the NO trapped by the cuprous center was being released then recaptured by the Fe^{II} (Scheme 4).

Given that trapping of NO by the ferrous complex would be expected to occur with near diffusion-limited second-order rate constants (~10^9 M^{-1} s^{-1}), the competitive trapping by Cu^{I} suggests that the rate constants for the NO reaction of these Cu^{I} centers are comparable. If the subsequent slower process is rate-limited by dissociation of NO from the Cu^{I}–NO center, the apparent rate constant (64 s^{-1} at 298 K) implies that the first-order NO dissociation rate constant is ~10^2 s^{-1}. These values give k_{on}/k_{off} = ~10^7 M^{-1} as an estimate overall equilibrium constant for Cu^{I}–NO bonding, which is substantial, but less than that typical for ferrous heme proteins and models.

Another metal-NO interaction of potential biological interest is the cobalt of vitamin B_{12}. The reduced (Co^{II}) form of aquacobalamin binds nitric oxide to yield the adduct Cbl(II)(NO) with an equilibrium constant of ~10^8 M^{-1} (25°C) [111]. Flash photolysis led to the transient disruption of this equilibrium followed by relaxation back to the equilibrium state. Varying the NO concentration allowed Wolak et al. [112] to determine the k_{on} for reforming the Co–NO bond as 7.4×10^8 M^{-1} s^{-1}, a value that is comparable to the second-order rate constants reported for reactions of free radicals with reduced cobalamin. The k_{off} value was determined by using Fe(EDTA) trapping of NO, and the resulting k_{on}/k_{off} ratio is, as it should be, in good agreement with the K_{14} value reported previously. Notably, while the cobalamin-NO interaction has drawn some interest, it is not clear what physiological role this might play.

$$\mathrm{Cbl(II)(H_2O) + NO \underset{k_{off}}{\overset{k_{on}}{\rightleftharpoons}} Cbl(II)(NO).} \tag{15}$$

A recent publication by Bakac et al. [113] has reported the results of flash photolysis and NO scavenger kinetics studies to determine the NO k_{on} and k_{off} values, respectively, for several other cobalt(II) macrocycle complexes and their rhodium(II) analogs as well as for the Cr(II) nitrosyl complex $Cr(H_2O)_5(NO)^{2+}$. These rate constants as well as literature values were then used to calculate the K_{NO} values for nitrosyl complex formation in solution, which were compared to K_{O2} values for formation of the analogous dioxygen complexes. The plot of log K_{NO} vs. log K_{O2} in 298 K aqueous solution proved to be linear with a unitary slope, indicating a direct correlation between the intrinsic bonding affinities of NO and O_2 for these metal centers. However, such a correlation would not carry over to the heme proteins given the huge differences in the affinities of O_2 and NO for soluble guanylyl cyclase and for myoglobin that can be attributed to the different interactions of the coordinated diatomic ligands with the protein amino acid residues [6].

In this section we have focused on the reactions of NO with Cu and Fe systems primarily by the reaction of these metal complexes with NO itself. However, there are other pathways to nitrosyl complexes. For example, nitrite reduction concomitant with (formal) oxidation of the metal can lead to a metal-nitrosyl complex illustrated in (16) [114–117].

$$\mathrm{L_xM^{n+} + NO_2^- + 2\ H^+ \rightleftharpoons L_xM(NO)^{(n+1)+} + H_2O.} \tag{16}$$

5 Reductive Nitrosylation and Other Reactions of Coordinated NO

Ligand-metal bonding generally involves electronic redistribution owing to the balance between ligand-to-metal σ- and π- donation and metal-to-ligand-backbonding. NO is especially versatile in this regard, as we have described above in Sect. 2. If there is charge transfer to the metal center resulting (formally) in a coordinated nitrosonium cation (NO^+), that species might have enhanced susceptibility to reactions with nucleophiles. On the other hand, if such charge transfer is in the opposite direction, the resulting coordinated nitroxyl anion NO^- may be susceptible to electrophilic attack. However, it is worth remembering that the nitrosyl typically undergoes reverse dissociation as a neutral NO, so assigning the oxidation states in this manner is rather arbitrary.

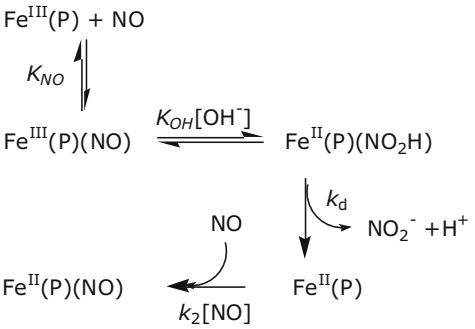

Scheme 5 Mechanism proposed by Hoshino et al. [122] for the reductive nitrosylation of selected ferriheme proteins (P = porphyrin ligand)

5.1 *Reactions of Iron(III) Nitrosyls with Nucleophiles*

Nucleophilic reactions with coordinated NO can be illustrated by the long-known reversible reaction of hydroxide with the nitrosyl ligand of the nitroprusside ion (NP) (17). The reaction rate is first order each in [OH^-] and in [$Fe(CN)_5(NO)^{2-}$] [118], so the likely reactive intermediate is the hydroxide adduct $Fe(CN)_5(N(O)OH)^{3-}$. The reaction is reversed in acidic solution. NP reacts with other nucleophiles such as mercaptans (RSH) and mercaptides (RS^-) to form deeply colored metal nitroso–thiolato intermediates [118]. These are unstable and decay via formation of disulfides and reduced NP, which subsequently decomposes by cyanide loss. Such reactions have physiological significance given that sodium nitroprusside has long been used as an intravenously administered vasodilator for hypertensive emergencies [119, 120].

$$Fe(CN)_5(NO)^{2-} + 2\ OH^- \rightleftharpoons Fe(CN)_5(NO_2)^{4-} + H_2O. \tag{17}$$

Facile nucleophilic attack at a coordinated nitrosyl is the likely mechanism for the NO reduction of metal centers. Ferric porphyrins have long been known to undergo such "reductive nitrosylation" in the presence of excess NO [47, 72, 121]. For example, when aqueous metHb is exposed to excess NO, the product is the ferrohemoglobin NO adduct, Hb(NO) (Scheme 5) [122]. Other ferriheme proteins such as cytochrome *c* (Cyt^{III}) and metMb are reduced by excess NO in aqueous solutions at pH values >7, but metHb is susceptible even at lower pH. The kinetics behavior for Cyt^{III} and metMb with regard to the NO concentration and the pH is consistent with the proposed base catalyzed mechanism shown in Scheme 5. However, it is important to recognize that the driving force of the reductive nitrosylation of the heme proteins and models at near neutral pH is the very great stability of the ferrous nitrosyl complexes formed under excess NO. In the absence of excess NO, the reverse reaction, namely, nitrite reduction by the ferrous complexes, is thermodynamically favored [117, 123].

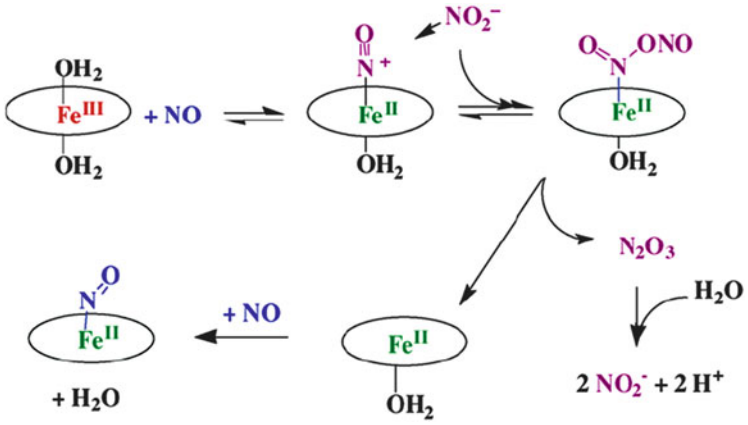

Scheme 6 Proposed mechanism for the nitrite catalysis of the reductive nitrosylation of Fe^{III}(TPPS), metHb, and metMb [127]

The nitrosyl complex of metMb has also been reported to react with the biological antioxidant glutathione GSH (in the presence of excess NO) to give Mb(NO) and *S*-nitrosoglutathione (GSNO) [124]. The GSH reaction with metMb(NO) is surprisingly facile, given that the smaller and more basic hydroxide ion is only an order of magnitude more reactive [122]. Nonetheless, this result points to the potential role of ferriheme nitrosyls acting as nitrosating agents toward biologically relevant nucleophiles [125, 126].

More recent studies by Fernandez et al. demonstrated that the reductive nitrosylations of Fe^{III}(TPPS) [127] and of metHb and metMb [128] are promoted by general base catalysis and by other nucleophiles, including nitrite ion (Scheme 6). In the case of the latter, the catalytic role of nitrite in promoting reductive nitrosylation of these ferric heme models and proteins was first discovered in an attempt to pin down experimental anomalies that were eventually attributed to the ubiquitous NO_2^- impurities in aqueous NO solutions.

The observation of nitrite catalysis of ferriheme nitrosyl reactions has generated considerable interest in the potential formation of N_2O_3 as an intermediate that might assume key biological roles [129, 130]. Receiving particular attention is the possibility that this reaction might explain the vasodilatory and other protective effects of nitrite ion in mammalian physiology [131, 132].

5.2 *Reduction of Copper(II) Complexes by NO*

The Cu(II) complex $Cu(dmp)_2(H_2O)^{2+}$ (dmp = 2,9-dimethyl-1,10-phenanthroline) is a stronger oxidant than most Cu(II) complexes (reduction potential = 0.58 V vs. NHE) [133]. Since the $Cu(phen)_2(H_2O)^{2+}$ analog (phen = 1,10-phenanthroline) is a much weaker oxidant (0.18 V), this property can be attributed to the steric

Scheme 7 Proposed mechanism for NO reduction of $Cu(dmp)_2(H_2O)^{2+}$ in buffer solution

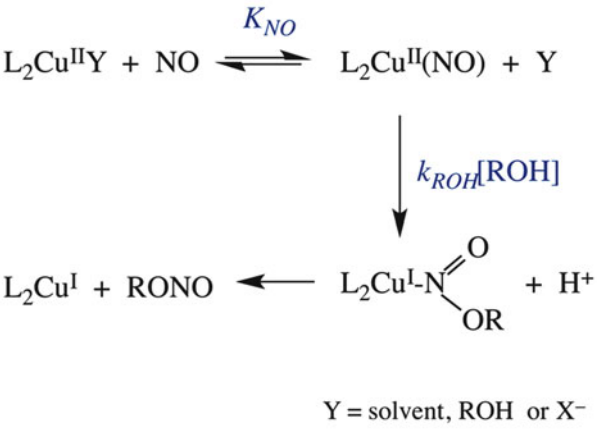

repulsion between the methyl groups of the respective dmp ligands that favors the tetrahedral coordination of Cu(I) over the tetragonal pyramidal structure of Cu(II).

In methanol, $Cu(dmp)_2(H_2O)^{2+}$ reacts with NO to give $Cu(dmp)_2^+$ and methyl nitrite (18); in water, the second product is NO_2^- [134]. In CH_2Cl_2, the reaction does not occur unless methanol is added. At a fixed pH, the kinetics in aqueous solution proved to be first order in [NO] and in $[Cu(dmp)_2(H_2O)^{2+}]$. Addition of a small concentration of $NaNO_2$ (5×10^{-5} M) had no effect, although at higher concentrations, various anions, including the conjugate bases of the buffers, inhibited the reaction. This inhibition was attributed to competition for the labile fifth coordination site of the Cu(II).

$$Cu(dmp)_2(H_2O)^{2+} + NO + ROH \rightarrow Cu(dmp)_2^{+} + RONO + H^+ + H_2O. \quad (18)$$

One prospective mechanism discussed for this reaction would be simple outer sphere electron transfer from NO to Cu(II) followed by hydrolysis of the resulting NO^+. Alternatively, a mechanism that is more consistent with the inhibition noted above and closer to those discussed above for NO reductions of the ferriheme proteins and models would be an inner sphere pathway such as illustrated in Scheme 7. The latter alternative gains credence from studies showing that NO reduction of the more sterically crowded, but stronger, oxidant $Cu(dpp)_2^{2+}$ (dpp = 2,9-diphenyl-1,10-phenanthroline) is slower under comparable conditions than the reduction of $Cu(dmp)_2(H_2O)^{2+}$ [135].

A somewhat different mechanism has prove necessary to interpret the reaction of NO with the Cu(II) complex $Cu(DAC)^{2+}$ (DAC = 1,8-bis (9-anthracylmethyl)(1,4,8,11-tetraaza-cyclotetradecane or bis(9-anthracylmethyl)-cyclam) [136, 137]. Although free DAC is fluorescent, analogous solutions of $[Cu(DAC)]^{2+}$ are not, owing to intramolecular quenching by the Cu(II) center. Introduction of NO to a methanolic solution of $Cu(DAC)^{2+}$ led to the disappearance of the characteristic weak *d–d* absorption band at 566 nm and to the appearance of

anthracene-type fluorescence. Cu(I) was detected electrochemically; however, in marked contrast to (18), the reduction of Cu(II) was accompanied by the *N*-nitrosation and release of the DAC ligand (19) as evidenced by ESI-mass spectral and ^{1}H-NMR analysis. It is this *N*-nitrosated DAC that is responsible for the strong luminescence.

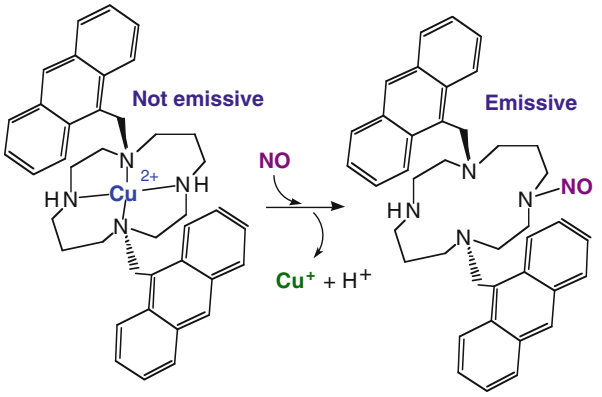

(19)

The rate of the reaction depicted in (19) is relatively slow in neutral aqueous media but is accelerated by base. Kinetic studies show it to be first order in the concentrations of $Cu(DAC)^{2+}$, NO, and OH^{-} [137]. Based on these observations, two mechanisms have been discussed. The first is analogous to Scheme 7 with the NO initially reacting at the Cu(II) site to form a Cu^{II}–NO (or Cu^{I}–NO^{+}) complex. This would be followed by deprotonation of one of the amines and NO^{+} migration to the resulting coordinated amide. Given that the DAC type ligand is well suited for square planar coordination to Cu(II) but is not well suited for tetrahedral coordination to Cu(I), the nitrosated ligand is then released. The other proposed mechanism involves NO attack at a coordinated amine that has been deprotonated. This step would lead directly to amine nitrosation and concomitant reduction of Cu(II) to Cu(I) (Scheme 8). This latter pathway is analogous to electron transfer between metal centers involving a bridging ligand, and DFT calculations suggest that this is the more favorable pathway [137].

Since reductions of metal centers by NO are generally thought to occur via nucleophilic attack at an activated M^{n+}-NO ($M^{(n-1)+}(NO^{+})$) species to give the nitroso-nucleophile product and the reduced metal center [72], there was little precedent for Scheme 8. An exception was the reaction of NO with $Ru(NH_3)_6^{3+}$ in alkaline media, which is reported to give the Ru(II) dinitrogen complex $Ru(NH_3)_5(N_2)^{2+}$ [70]. Given that the latter reaction leads to the formation of an N–N bond, it is likely that it is proceeding by NO attack on a coordinated amide ligand [72] with concomitant reduction of the metal center. Such a mechanism for the nitrosation of coordinated ligands may have broader implications. For example, it was reported by Montfort et al. [138] that reaction of excess NO with bedbug nitrophorin leads to nitrosylation and reduction of the heme iron as well as to

Scheme 8 Prospective inner sphere electron transfer mechanism for the NO reduction of $Cu(DAC)^{2+}$

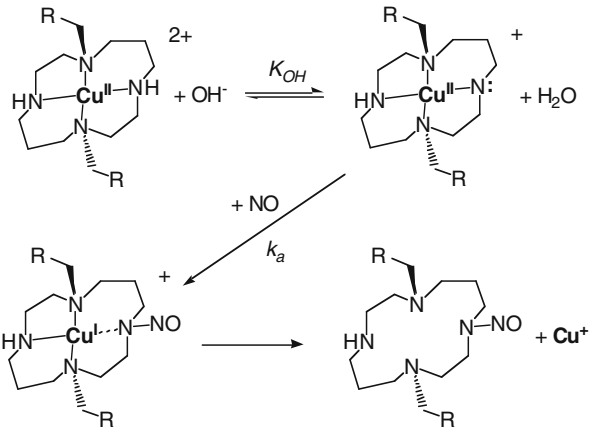

nitrosation of the proximal cysteinate ligand (cys-60). Similarly, van Eldik et al. [139] described the reaction of a nitrosyl ferriheme thiolate complex with NO to form $Fe^{II}(Por)(NO)$ and RS–NO (20). While these reactions could occur via homolytic Fe–SR cleavage followed by trapping of RS• by NO, an alternative could be NO attack at the coordinated thiolate ligand in analogy to the NO reduction of $Cu(DAC)^{2+}$. Furthermore, it is notable that the NO reaction with a coordinated thiolate is the microscopic reverse of the decomposition of *S*-nitrosothiols catalyzed by copper(I) [140], a reaction that is likely to proceed via the initial coordination of Cu(I) at the RSNO sulfur followed by homolytic dissociation of the RS–NO bond [141].

$$\mathrm{Fe(Por)(NO)(SR)} + \mathrm{NO} \rightarrow \mathrm{Fe(Por)(NO)} + \mathrm{RSNO}. \tag{20}$$

For some time, there has been an interest in possible utilization of the NO reduction of coordinated metal complexes of luminescent ligands as turn-on sensors for NO detection [142, 143]. In this context, it is of interest that in weakly coordinating solvents, the cuprous complex $Cu(dmp)_2^+$ is strongly luminescent from its metal-to-ligand charge transfer (MLCT) state(s), while the Cu(II) analog is not [144]. However, since the MLCT emission from $Cu(dmp)_2^+$ is strongly quenched by nucleophiles, including H_2O and CH_3OH, the reaction depicted by (18) would not be an effective NO sensor, so another approach was needed. This was a stimulus for exploring the reactions of $Cu(DAC)^{2+}$, since free ligand DAC is luminescent from its anthracene chromophores, but its emission is nearly completely quenched in Cu $(DAC)^{2+}$. The reaction of NO with $Cu(DAC)^{2+}$ did lead to strongly enhanced luminescence, the emissive luminophore being the nitrosated DAC; however, the reaction was considered to be too slow at physiological pH to be of practical application. Lim et al., however, saw greater potential in analogous systems and were able to build sensitive NO sensors using CuL_2^{2+}, where L is a bidentate ligand such as dansyl ethylenediamine or dansyl aminomethylpyridine [145], or $Cu^{II}(Cl)(FL)$, where FL is a tridentate metal chelating ligand

modified with a pendant fluorescein [146]. In each case NO reduction of the Cu (II) center leads to strongly enhanced ("turned on") emission from the ligands. In the case of FL the luminophore product is the *N*-nitrosated FL–NO (21), which is actually more fluorescent ($\Phi_F = 0.58$) than FL itself ($\Phi_F = 0.08$) owing to suppression of electron transfer fluorescence quenching involving the free amine functionality [147]. Cu^{II}(Cl)(FL) has been utilized as a NO sensor in cell cultures and tissue. Notably, a quantitative study of the NO reduction of Cu^{II}(Cl)(FL) found the rate to be first order in [Cu^{II}(Cl)(FL)], [OH^-], and [NO] as seen for $Cu(DAC)^{2+}$ [137], and an inner sphere mechanism in analogy to Scheme 8 was proposed [147].

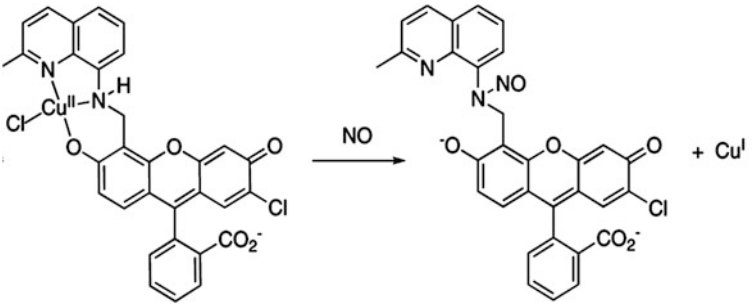

(21)

Mondal and coworkers have also prepared similar sensors with copper(II) coordinated by tridentate ligands with pendent dansyl groups that become much more fluorescent when the Cu(II) is reduced by NO in methanol [148]. In this case, however, the ligand was not nitrosated, so a mechanism along the lines of Scheme 7 is likely, although there was no direct evidence for the formation of a $Cu^{II}NO$ intermediate. Previous studies by this research group with other ligands did observe ligand nitrosation occurring concomitant with NO reductions of Cu(II) complexes [149]. In another interesting study [150], these researchers prepared the cupric complexes $Cu(2\text{-aminomethylpyridine})_2^{2+}$ and $Cu(tren)(AN)^{2+}$ (tren = bis-(2-aminoethyl)amine, AN = acetonitrile). When an acetonitrile solution of the former complex was purged with NO, immediate changes in the absorption spectra (shifts in the LF band from 582 to 660 nm) were apparent, and the solution became EPR silent. A similar pattern was seen with $Cu(tren)(AN)^{2+}$. This was followed by a slow reaction to form the final products, which were Cu(I) plus species apparently formed by the diazotization of the ligand primary amines. The FTIR spectrum of the transient species showed a strong new band at 1,642 cm^{-1} that was attributed to the ν_{NO} of a transient $Cu^{II}L_2(NO)^{2+}$ complex. However, this ν_{NO} occurred nearly 300 cm^{-1} lower frequency than that of the structurally characterized Cu^{II}(NO) complex reported by Hayton and coworkers [41], so the difference is puzzling.

The redox chemistry between NO and Cu^{2+} has also been invoked as being important to the biological function of the multi-copper blood protein ceruloplasmin, which has been termed a "nitric oxide oxidase" [151]. It was proposed that ceruloplasmin is an NO oxidase that helps to maintain the homeostasis between nitrite and NO in mammalian blood by converting NO to NO_2^-.

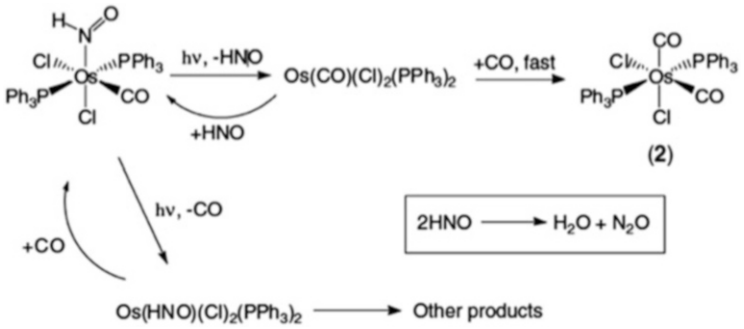

Scheme 9 Competitive CO and HNO photodissociation from $Os(CO)Cl_2(PPh_3)_2(HNO)$ [154]

5.3 *Protonation of Metal Nitrosyls*

An important form of electrophilic attack on metal nitrosyls is protonation. An early example of which is the reversible reaction of HCl with the osmium compound $Os(CO)Cl(PPh_3)_2(NO)$ to give the first structurally characterized N-coordinated HNO complex $Os(CO)Cl_2(PPh_3)_2(HNO)$ (Scheme 9) [152, 153]. Subsequent studies by Marhenke et al. [154] demonstrated that photolysis of the latter compound led competitive reversible dissociation of CO and of HNO (Scheme 9).

A more biologically relevant example of M–NO protonation is the electrochemical reduction/protonation of Mb(NO) demonstrated by Farmer and coworkers [155]. Surfactant Mb(NO) films deposited on the graphite electrodes were shown to undergo reduction to $Mb(NO^-)_{surface}$ ($E_{1/2} = -0.63$ V vs. NHE) accompanied by protonation to give $Mb(HNO)_{surface}$. At more negative potentials, the latter was reported to undergo catalytic reaction with excess NO in solution to give N_2O. When Mb(HNO) was subsequently prepared in solution by reducing Mb(NO) with Cr^{2+}, the nitroxyl proton was observable by ^1H NMR as a singlet at 14.8 ppm [155].

Olabe and coworkers [156] have shown that the nitroprusside ion $Fe(CN)_5(NO)^{2-}$ can be sequentially reduced by two electrons in aqueous solution. The product of the second reduction $Fe(CN)_5(NO)^{4-}$ undergoes protonation (pK_a 7.7) to give an N-coordinated HNO complex (22) that is remarkably stable. The stability of $Fe(CN)_5(NO)^{4-}$ clearly points to the NO functionality as being the site of the second reduction, and this complex can be considered to be a low-spin d^6 Fe(II) complex of the nitroxyl anion, that is, a $Fe^{II}(NO^-)$ species. If instead the second electron was localized on the metal, the resulting low-spin d^7 complex should be very labile toward ligand substitution. The proton NMR spectrum shows a proton resonance at 20.02 ppm that splits into a doublet when ^{15}NO-labeled nitroprusside was used.

$$Fe(CN)_5(NO)^{4-} + H^+ \rightleftharpoons Fe(CN)_5(HNO)^{3-}. \tag{22}$$

The osmium, reduced myoglobin, and reduced nitroprusside cases described above each involve protonation of a $\{MNO\}^8$ complex. A different example has recently been reported where a $\{MNO\}^7$ complex displays a tendency to decompose slowly in aqueous solution presumably via protonation of the nitrosyl followed by dissociation of HNO. In this case, the complex was the water-soluble heme model Fe^{II}(TPPS)(NO) that had been prepared in slightly acidic (pH 5.8) aqueous buffer [149]. Although, such ferrous porphyrinato nitrosyls are often considered to be quite unreactive, this solution slowly underwent spontaneous decay to give the ferric species Fe^{III}(TPPS) (23). The possible formation of HNO was first suggested by the observation of N_2O as a reaction product [157] (free HNO readily dimerizes to nitrous oxide) [158, 159] and was later demonstrated by direct observation using an HNO-specific electrochemical technique [61]. The proposal that this occurs via protonation (effectively an oxidative addition of H^+) followed by dissociation of HNO was based on the pH-dependence of the reaction.

$$Fe^{II}(TPPS)(NO) + H^+ \rightleftharpoons Fe^{III}(TPPS)(HNO) \rightarrow Fe^{III}(TPPS) + HNO. \quad (23)$$

The chemistry of HNO and the formation and reactions of HNO metal complexes have been extensively reviewed [158–161].

5.4 Reactions with Dioxygen

Reactions with O_2 represent some of the most important processes involving NO under physiological conditions. Nitric oxide autoxidation that is not mediated by metal centers has been shown to display third-order kinetics (24) whether in the gas phase, in aprotic solvents or in aqueous media [162]. The fact that this reaction rate is second order in [NO] is particularly significant in the biological context. Under the very low concentrations (nanomolar) where NO is an important signaling agent, such as in blood pressure control, the reaction with oxygen is very slow. In contrast, at the higher concentrations that are typical of induced NO production during immune response to pathogens, the autoxidation process may play important physiological roles, such as the generation of cytotoxic nitrogen oxides like N_2O_3.

$$-d[NO]/dt = k_{aut}[NO]^2[O_2]. \quad (24)$$

Notably, there are differences in the products observed in aqueous vs. non-aqueous media and this may also have biological relevance. NO autoxidation in aqueous solution leads to the formation of nitrous acid according to the stoichiometry shown in (25) [163]. In contrast, the autoxidation product in aprotic media is nitrogen dioxide, which is a much stronger oxidant toward cellular components [164, 165]. Aprotic autoxidation may have particular relevance biologically owing to the higher solubility of both NO and O_2 in hydrophobic media. As a consequence

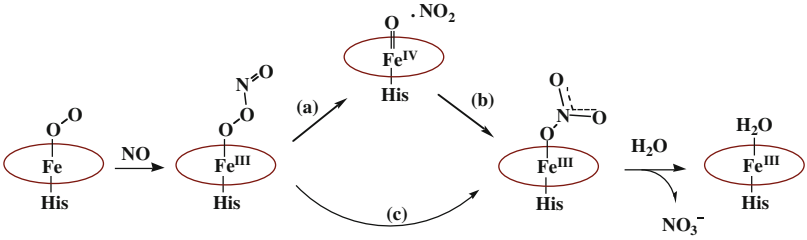

Scheme 10 Hypothetical pathways leading to the dioxygenation of NO by $Mb(O_2)$ or $Hb(O_2)$ [171]

of reactant partitioning between cellular hydrophobic and hydrophilic regions and the third-order kinetics, a disproportionate fraction of autoxidation may occur in hydrophobic regions to give NO_2 as a key intermediate at these locations [166].

$$4NO + O_2 + 2H_2O \rightarrow 4H^+ + 4NO_2^-. \tag{25}$$

The reactivity of NO with O_2 is dramatically affected by coordination of one or the other of these reactants to a metal center. For example, dioxygenation of NO by oxymyoglobin (e.g. (26)) or by oxyhemoglobin is quite fast and occurs by a rate law that is first order in NO concentration (e.g., $-d[NO]/dt = k_2[NO][Mb(O_2)]$, $k_2 = >10^7\ M^{-1}\ s^{-1}$ at pH 7) [167, 168]. Furthermore, the NO_x product is nitrate (NO_3^-), not nitrite or nitrogen dioxide, and the other product is metMb. Such reactions are generally considered to be important sinks that scavenge NO in the cardiovascular system [169].

$$NO + Mb(O_2) \rightarrow metMb + NO_3^-. \tag{26}$$

Mechanistically, given that the O_2 bound to the iron of myoglobin or hemoglobin is considered to have superoxide character, the rapid reaction with the free radical NO is not surprising. Since the product of solution phase reaction of free O_2^- with NO is the peroxynitrite ion $OONO^-$, one might expect that the first species formed in the NO reaction with oxymyoglobin would be the corresponding peroxynitrite complex (Scheme 10). This reaction has been the subject of several fast-flow spectroscopic studies, and while earlier studies claimed to have observed this intermediate, later ones concluded that the first species observable is the nitrate complex $Fe^{III}(NO_3^-)$ [170]. In this context, Kurtikyan et al. [171] used low-temperature matrix spectroscopy to probe the reaction of the heme model $Fe^{II}(TPP)(O_2)$ (TPP^{2-} = tetraphenylporphyrinato dianion) with NO. Even at 100 K, the purported peroxynitrite intermediate $Fe^{III}(TPP)(OONO^-)$ was not observable, so it was concluded that once this species is formed, it must decay very rapidly to the more stable nitrate complex $Fe^{III}(TPP)(NO_3^-)$. Notably, different computational approaches also disagree on the potential stability of that intermediate [172, 173].

Superficially, the reaction of O_2 with nitrosyl myoglobin Mb(NO) (27) appears similar to that of NO with $Mb(O_2)$. This reaction has been studied in detail by Skibsted and coworkers [174], owing in part to its importance to the stability of cured meat. The same products, metMb and NO_3^-, are formed; however, the oxygenation of Mb(NO) is very much slower and follows a different rate law. Indeed several kinetics studies [174, 175] indicated the operation of two slow (pseudo) first-order processes under an oxygen atmosphere with different activation parameters, one of the two being modestly dependent on the O_2 concentration. However, under one atm of O_2 at 30°C, the two rate constants were nearly the same, $\sim 6 \times 10^{-4}$ s^{-1}. Notably, these values are close to the rate of spontaneous NO dissociation from Mb(NO), and one of these was indeed attributed to NO dissociation followed by O_2 trapping of the resulting Mb to give $Mb(O_2)$, which then reacts rapidly with NO according to (27) [174]. The efficiency of this step would be enhanced by containment of NO in the hydrophobic pockets of the protein. For the second kinetically detected process, it was suggested that O_2 plays a role in labilizing the NO, although it is still dominated by dissociation. The reaction is also markedly accelerated by light [176], consistent with the thermal autoxidation of Mb(NO) being dominated by NO dissociation.

$$O_2 + \text{Mb(NO)} \rightarrow \text{metMb} + NO_3^-. \tag{27}$$

6 Summary

This chapter has provided a brief review of NO reactions with metal centers and our principal focus has been on studies where quantitative photochemical and thermal kinetics techniques have been used to probe reactions that may play key roles in the biological activity of NO. As a consequence, we have concentrated principally on reactivity involving iron and copper metal centers, but even with this approach, it was necessary to leave out numerous topics relevant to chemists and chemical biologists owing to the volume of information regarding the chemistry, biochemistry, and pathobiology of NO. For example, NO is a reversible inhibitor of the critical redox protein cytochrome *c* oxidase, which contains both hemes and a redox-active copper site [177]. Furthermore, other closely related species such as HNO and nitrite are drawing considerable attention as being key components of the larger picture. Nonetheless, we can reemphasize certain important general patterns. The first is that NO is a stable free radical that reacts readily with other free radicals and redox-active metal centers, especially if the latter are substitution labile. For example, mammalian blood pressure regulation by NO centers on the rapid reaction with the ferroheme site of sGC, and this process must be fast with a large formation constant if the low NO concentrations generated are to be effective. Key biological roles not only involve formation and decay of nitrosyl complexes but also how NO coordination affects the reactivities of the metal and other ligands and how the

metal mediates the chemistry of the coordinated NO. Understanding the dynamics, thermodynamics, and mechanisms of the relevant fundamental processes provides insight into how the chemical biology of NO and other relevant nitrogen oxides function.

Acknowledgements Reactivity studies of nitrogen oxides in the UCSB laboratory of PCF have long been supported by the Division of Chemistry of the US National Science Foundation (Current grant CHE-1058794). JCMP thanks Coordenação de Aperfeiçoamento de Pessoal de Nível Superior (CAPES) for fellowship support.

References

1. Ignarro LJ (1999) Angew Chemie I Ed 38:1882
2. Furchgott RF (1999) Angew Chemie I Ed 38:1870
3. Murad F (1999) Angew Chemie I Ed 38:1856
4. Ignarro LJ (2010) Nitric oxide: biology and pathobiology. 2nd edn. Elsevier Inc., Burlington
5. Bellamy TC, Garthwaite J (2001) J Biol Chem 276
6. Boon EM, Huang SH, Marletta MA (2005) Nature Chem Biol 1:53
7. Griffith OW, Stuehr DJ (1995) Ann Rev Physiol 57:707
8. Greenwood NN, Earnshaw A (1993) Chemistry of the elements. Pergamon, Oxford, Chapter 11
9. Coppens P, Novozhilova I, Kovalevsky A (2002) Chem Rev 102:861
10. Novozhilova IV, Coppens P, Lee J, Richter-Addo GB, Bagley KA (2006) J Am Chem Soc 128:2093
11. Tocheva EI, Rosell FI, Mauk AG, Murphy MEP (2004) Science 304:867
12. Tocheva EI, Rosell FI, Mauk AG, Murphy MEP (2007) Biochemistry 46:12366
13. Merkle AC, Lehnert N (2012) Dalton Trans 41:3355
14. Periyasamy G, Sundararajan M, Hillier IH, Burton NA, McDouall JJW (2007) Phys Chem 9:2498
15. Mingos DMP (1973) Inorg Chem 12:1209
16. Enemark JH, Feltham RD (1974) Coord Chem Rev 13:339
17. Wyllie GRA, Scheidt WR (2002) Chem Rev 102:1067
18. Copeland DM, Soares AS, West AH, Richter-Addo GB (2006) J Inorg Biochem 100:1413
19. Cohn JN, McInnes GT, Shepherd AM (2011) J Clin Hyperten 13:690
20. Roussin J (1858) Ann Chim Phys 52:285
21. Rauchfuss TB, Weatherill TD (1982) Inorg Chem 21:827
22. Mokh VP, Poltorakov AP, Serezhenkov VA, Vanin AF (2010) Nitric Oxide Biol Chem 22:266
23. Flitney FW, Megson IL, Thomson JLM, Kennovin GD, Butler AR (1996) Br J Pharmacol 117:1549
24. Bourassa J, DeGraff W, Kudo S, Wink DA, Mitchell JB, Ford PC (1997) J Am Chem Soc 119:2853
25. Kudo S, Bourassa JL, Boggs SE, Sato Y, Ford PC (1997) Analyt Biochem 247:193
26. Conrado CL, Bourassa JL, Egler C, Wecksler S, Ford PC (2003) Inorg Chem 42:2288
27. Wecksler SR, Mikhailovsky A, Korystov D, Ford PC (2006) J Amer Chem Soc 128:3831
28. Zheng Q, Bonoiu A, Ohulchanskyy TY, He GS, Prasad PN (2008) Mol Pharm 5:389
29. Chen TN, Lo FC, Tsai ML, Shih KN, Chiang MH, Lee GH, Liaw WF (2006) Inorg Chim Acta 359:2525
30. Kim YM, Chung HT, Simmons RL, Billiar TR (2000) J Biol Chem 275:10954

31. Butler AR, Megson IL (2002) Chem Rev 102:1155
32. Bosworth CA, Toledo JC Jr, Zmijewski JW, Li Q, Lancaster JR Jr (2009) Proc Natl Acad Sci USA 106:4671
33. Tonzetich ZJ, McQuade LE, Lippard SJ (2010) Inorg Chem 49:6338
34. Hickok JR, Sahni S, Shen H, Arvind A, Antoniou C, Fung LWM, Thomas DD (2011) Free Radic Biol Med 51:1558
35. Manoharan PT, Hamilton WC (1963) Inorg Chem 2:1043
36. Lu TT, Tsou CC, Huang HW, Hsu IJ, Chen JM, Kuo TS, Wang Y, Liaw WF (2008) Inorg Chem 47:6040
37. Bryar TR, Eaton DR (1992) Canad J Chem 70:1917
38. Johansson G, Lipscomb WN (1957) J Chem Phys 27:1417
39. Ruggiero CF, Carrier SM, Antholine WE, Whitataker JW, Cramer CJ, Tolman WB (1993) J Am Chem Soc 115:11285
40. Fujisawa K, Tateda A, Miyashita Y, Okamoto K, Paulat F, Praneeth VKK, Merkle A, Lehnert N (2008) (I) J Am Chem Soc 130:1205
41. Wright AM, Wu G, Hayton TW (2010) J Am Chem Soc 132:14336
42. Scheidt WR, Frisse ME (1975) J Am Chem Soc 97:17
43. Nasri H, Haller KJ, Wang Y, Huynh BH, Scheidt WR (1992) Inorg Chem 31:3459
44. Scheidt WR, Brinegar AC, Ferro EB, Kerner JF (1977) J Am Chem Soc 99:7315
45. Brucker EA, Olson JS, Ikeda-Saito M, Philips GN Jr (1998) Proteins Struct Funct Genet 30:352
46. Chan NL, Kavanaug JS, Rogers PH, Arnone A (2004) Biochemistry 43:118
47. Wayland BB, Olson LW (1974) J Am Chem Soc 95:6037
48. Hoffman BM, Weschler CJ, Basolo F (1976) J Am Chem Soc 98:5473
49. Palmer G (1979) In: Dolphin D (ed) The porphyrins, vol 4. Academic, New York, Chap. 6
50. Gouterman M (1961) J Mol Spectrosc 6:138
51. Westcott BL, Enemark JH (1999) In: Solomon EI, Lever ABP (eds) Inorganic electronic structure and spectroscopy, vol 2. Wiley, New York pp 403–450
52. Scheidt WR, Hatano K, Rupprecht GA, Piciulo PL (1979) Inorg Chem 18:292
53. Traylor TG, Sharma VS (1992) Biochemistry 31:2847
54. Perutz MF, Kilmartin JV, Nagai K, Szabo A, Simon SR (1976) Biochem 15:378
55. Dierks EA, Hu S, Vogel KM, Yu AE, Sprio TG, Burstyn JN (1997) J Am Chem Soc 119:7316
56. Derbyshire ER, Marletta MA (2012) Ann Rev Biochem 81:559
57. Patterson JC, Lorkovic IM, Ford PC (2003) Inorg Chem 42:4902
58. Toledo JC, Silva HAS, Scarpellini M, Mori V, Camargo AJ, Bertotti M, Franco DW (2004) Eur J Inorg Chem 1879
59. Goodrich LE, Paulat F, Praneeth VKK, Lehnert N (2010) Inorg Chem 49:6293
60. Caramori GF, Kunitz AG, Andriani KF, Doro FG, Frenking G, Tfouni E (2012) Dalton Trans 41:7327
61. Heinecke JL, Khin C, Pereira JCM, Suárez SA, Iretskii AV, Doctorovich F, Ford PC (2013) J Am Chem Soc 135:4007
62. Conradie J, Hopmann KH, Ghosh A (2010) J Phys Chem B 114:8517
63. Olson JS, Phillips GN (1996) J Biol Chem 271:17593
64. Strickland N, Harvey JN (2007) J Phys Chem B 111:841
65. Praneeth VKK, Paulat F, Berto TC, George SD, Näther C, Sulok CD, Lehnert N (2008) J Am Chem Soc 130:15288
66. Walda KN, Liu XY, Sharma VS, Magde D (1994) Biochem 33:2198
67. Benabbas A, Ye X, Kubo M, Zhang ZY, Maes EM, Montfort WR, Champion PM (2010) J Am Chem Soc132:2811
68. Park J, Lee T, Park J, Lim M (2013) J Phys Chem B 117:2850
69. Armor JN, Scheidegger HA, Taube H (1973) J Am Chem Soc 90:1968
70. Armor JN, Pell SD (1973) J Am Chem Soc 95:7625
71. Czap A, van Eldik R (2003) Dalton Trans 32:665

72. Ford PC, Fernandez BO, Lim MD (2005) Chem Rev 105:2439
73. Moore EG, Gibson QH (1976) J Biol Chem 251:2788
74. Tamura M, Kobayashi K, Hayashi K (1978) FEBS Let 88:124
75. Hoffman BM, Gibson QH (1978) Proc Natl Acad Sci USA 75:21
76. Rose EJ, Hoffman BM (1983) J Am Chem Soc 105:2866
77. Hoshino M, Arai S, Yamaji M, Hama Y (1986) J Phys Chem 90:2109
78. Ionascu D, Gruia F, Ye X, Yu A, Rosca F, Beck C, Demidov A, Olson JS, Champion PM (2005) J Am Chem Soc 127:16921
79. Purwar N, McGarry JM, Kostera J, Pacheco AA, Schmidt M (2011) Biochemistry 50:4491
80. Hoshino M, Kogure M (1989) J Phys Chem 93:5478
81. Hoshino M, Ozawa K, Seki H, Ford PC (1993) J Am Chem Soc 115:9568
82. Laverman LE, Ford PC (2001) J Am Chem Soc 123:11614
83. Laverman LE, Wanat A, Oszajca J, Stochel G, Ford PC, van Eldik R (2001) J Am Chem Soc 123:285
84. Ford PC (2010) Inorg Chem 49:6226
85. Wolak M, van Eldik R (2005) J Am Chem Soc 127:13312
86. Abu-Soud HM, Ichimori K, Presta A, Stuehr DJ (2000) J Biol Chem 275:17349
87. Scheele JS, Bruner E, Kharitonov VG, Martasek P, Roman LJ, Masters BS, Sharma VS, Magde D (1999) J Biol Chem 274:13105
88. Andersen JF, Ding XD, Balfour C, Shokhireva TK, Champagne DE, Walker FA, Montfort WR (2000) Biochem 39:10118
89. Ouellet H, Lang J, Couture MR, Ortiz de Montellano P (2009) Biochem 48:863
90. Franke A, Stochel G, Jung C, Van Eldik R (2004) J Am Chem Soc 126:4181
91. Kharitonov VG, Russwurm M, Madge D, Sharma VS, Koesling D (1997) Biochem Biophys Res Comm 239:284
92. Quaroni LG, Seward HE, McLean KJ, Girvan HM, Ost, TWB, Noble MA, Kelly SM, Price NC, Cheesman MR, Smith WE, Munro AW (2004) Biochem 43:16416
93. Rinaldo S, Arcovito A, Brunori M, Cutruzzolà F (2007) J Biol Chem 282:14761
94. Kakar S, Hoffman FG, Storz JF, Fabian M, Hargrove MS (2010) Biophys Chem152:1
95. Abbruzzetti S, Faggiano S, Spyrakis F, Bruno S, Mozzarelli A, Astegno A, Dominici P, Viappiani C (2011) IUBMB Life 63:1094
96. Condorelli P, George SC (2001) Biophys J 80:2110
97. Ostrich IJ, Gordon L, Dodgen HW, Hunt JP (1980) Inorg Chem 19:619
98. Schneppensieper T, Zahl A, van Eldik R (2001) Angew Chemie Int Ed Eng 40:1678
99. Hickok JR, Vasudevan D, Thatcher GRJ, Thomas DD (2012) Antioxi Redox Sig 17:962
100. Nhut G T, Kalyvas H, Skodje KM, Hayashi T, Moenne-Loccoz P, Callan PE, Shearer J, Kirschenbaum LJ, Kim E (2011) J Am Chem Soc 133 5 1184
101. Lin ZS, Lo FC, Li CH, Chen CH, Huang WN, Hsu IJ, Lee JF, Horng JC, Liaw WF (2011) Inorg Chem 50:10417
102. Vanin AF (2009) Nitric Oxide Biol Chem 21:1
103. Tonzetich ZJ, Do LH, Lippard SJ (2009) J Am Chem Soc 131:7964
104. Bourassa JL, Ford PC (2000) Coord Chem Rev 200:887
105. Sanina NA, Syrtsova LA, Shkondina NI, Rudneva TN, Malkova ES, Bazanov TA, Kotel'nikov AI, Aldoshin SM (2007) Nitric Oxide Biol Chem 16:181
106. Bourassa J, Lee B, Bernhard S, Schoonover J, Ford PC (1999) Inorg Chem 38:2947
107. Vanin AF, Papina AA, Serezhenkov VA, Koppenol WH (2004) Nitric Oxide 10:60
108. Wanat A, Schneppensieper T, Stochel G, van Eldik R, Bill E, Wieghardt K (2002) Inorg Chem 41:2
109. Schneppensieper T, Wanat A, Stochel G, Goldstein S, Meyerstein D, van Eldik R (2001) Euro J. Inorg Chem 2317
110. Lucas HR, Meyer GJ, Karlin KD (2009) J Am Chem Soc 131:13924
111. Zheng D, Birke R (2001) J Am Chem Soc 123:4637

112. Wolak M, Zahl A, Schneppensieper T, Stochel G, van Eldik R (2001) J Am Chem Soc 123:9780
113. Bakac A, Pestovsky O, Durfey BL, Kristian KE (2013) Chem Sci 4:2185
114. Gladwin MT, Grubina R, Doyle MP (2009) Accts Chem Res 42:157
115. He C, Knipp M (2009) J Am Chem Soc 131:12042
116. Yi J, Heinecke J, Tan H, Ford PC, Richter-Addo GB (2009) J Am Chem Soc 131:18119
117. Heinecke J, Ford PC (2010) Coord Chem Rev 254:235
118. Olabe JA (2008) Dalton Trans 3633
119. Cohn JN, McInnes GT, Shepherd AMJ (2011) Clin Hyperten 13:690
120. Vaughan CJ, Delanty N (2000) Lancet 356:411
121. Ascenzi P, Pesce A, Nardini M, Bolognesi M, Ciaccio C, Coletta M, Dewilde S (2013) Biochem Biophys Res Comm 430:1301
122. Hoshino M, Maeda M, Konishi R, Seki H, Ford PC (1996) J Am Chem Soc 118:5702
123. Koppenol WH (2012) Inorg Chem 51:5637
124. Reichenbach G, Sabatini S, Palombari R, Palmerini CA (2001) Nitric Oxide 5:395
125. Luchsinger BP, Rich EN, Gow AJ, Williams EM, Stamler JS, Singel DJ (2003) Proc Natl Acad Sci USA 100:461
126. Broniowska KA, Keszler A, Basu S, Kim-Shapiro DB, Hogg N (2012) Biochem J 442:191
127. Fernandez BO, Lorkovic IM, Ford PC (2004) Inorg Chem 43:5393
128. Fernandez BO, Ford PC (2003) J Am Chem Soc 125:10510
129. Basu S, Grubina R, Huang J, Conradie J, Huang Z, Jeffers A, Jiang A, He X, Azarov I, Seibert R, Mehta A, Patel R, King SB, Hogg N, Ghosh A, Gladwin MT, Kim-Shapiro DB (2007) Nature Chem Biol 3:785
130. Tejero J, Basu S, Helms C, Hogg N, King SB, Kim-Shapiro DB, Gladwin MT, Low NO (2012) J Biol Chem 287:18262
131. Lundberg J, Weitzberg E, Gladwin MT (2008) Nat Rev Drug Discov 7:156
132. Feelisch M, Fernandez BO, Bryan NS, Garcia-Saura MF, Bauer S, Whitlock DR, Ford PC, Janero DR, Rodriguez J, Ashrafian H (2008) J Biol Chem 283:33927
133. Lei Y, Anson FC (1994) Inorg Chem 33:5003
134. Tran D, Shelton BW, White Al. H, Laverman LE, Ford PC (1998) Inorg Chem 37:2505
135. Lim MD, Capps KB, Karpishin TB, Ford PC (2005) Nitric Oxide 12:244
136. Tsuge K, DeRosa F, Lim MD, Ford PC (2004) J Am Chem Soc 126:6564
137. Khin C, Lim MD, Tsuge K, Iretskii A, Wu G, Ford PC (2007) Inorg Chem 46:9323
138. Weichsel W, Maes EM, Andersen JF, Valenzuela JG, Shokhireva TK, Walker FA, Montfort WR (2005) Proc Natl Acad Sci USA 102:594
139. Franke A, Stochel G, Suzuki N, Higuchi T, Okuzono K, van Eldik R (2005) J Am Chem Soc 127:5360
140. Dicks AP, Swift HR, Williams DL, H, Butler AR, Al-Sa'doni HH, Cox BG (1996) J Chem Soc Perkin Trans 2:481
141. Melzer Marie M, Mossin S, Cardenas AJP, Williams KD, Zhang S, Meyer K, Warren TH (2012) Inorg Chem 5:8658
142. Franz KJ, Singh N, Lippard SJ (2000) Angew Chem I E 39:2120
143. Riklin M, Tran D, Bu X, Laverman LE, Ford PC (2001) JCS Dalton Trans 1813:1819
144. McMillin DR, Kirchoff JR, Goodwin KV (1985) Coord Chem Rev 64:83
145. Lim MH, Lippard SJ (2005) J Am Chem Soc 127:12170
146. Lim MH, Xu D, Lippard (2006) SJ Nat Chem Biol 2:375
147. McQuade LE, Pluth MD, Lippard SJ (2010) Inorg Chem 49:8025
148. Kumar P, Kalita A, Mondal B (2012) Dalton Trans 41:10543
149. Sarma M, Kalita A, Kumar P, Mondal B (2010) J Am Chem Soc 132:7846
150. Sarma M, Mondal B (2011) Inorg Chem 50:3206
151. Shiva S, Wang X, Ringwood LA, Xu X, Yuditskaya S, Annavajjhala V, Miyajima H, Hogg N, Harris ZL, Gladwin MT (2006) Nature Chem Biol 2:486
152. Grundy KR, Reed CA, Roper WR (1970) Chem Commun 1501

153. Wilson RD, Ibers JA (1979) Inorg Chem 18:336
154. Marhenke J, Joseph CA, Corliss MZ, Dunn T, Ford PC (2007) Polyhedron 26:4638
155. Lin R, Farmer PJ (2000) J Am Chem Soc 122:2393
156. Montenegro AC, Amorebieta VT, Slep LD, Martin DF, Roncaroli F, Murgida DH, Bari SE, Olabe JA (2009) Angew Chem Int Ed 48:4213
157. Khin C, Heinecke JL, Ford PC (2008) J Am Chem Soc 130:13830
158. Smith PAS, Hein GE (1960) J Am Chem Soc 82:5731
159. Miranda KM (2005) Coord Chem Rev 249:433
160. Doctorovich F, Bikiel D, Pellegrino J, Suarez SA, Larsen A, Marti MA (2011) Coord Chem Rev 255:2764
161. Fukuto JM, Cisneros CJ, Kinkade RL (2013) J Inorg Biochem 118:201
162. Ford PC, Wink DA, Stanbury DM (1993) FEBS Lett 326:1
163. Wink DA, Darbyshire JF, Nims RW, Saveedra JE, Ford PC (1993) Chem Res Toxicol 6:23
164. Silkstone RS, Mason MG, Nicholls P, Cooper CE (2012) Free Rad Biol Med 52:80
165. Ford E, Hughes MN, Wardman P (2002) Free Rad Biol Med 32:1314
166. Liu X, Miller MJS, Joshi MS, Thomas DD, Lancaster JR Jr (1998) Proc Natl Acad Sci USA 95:2175
167. Doyle MP, Hoekstra JW (1981) J Inorg Biochem14:351
168. Herold S, Exner M, Nauser T (2001) Biochemical 40:3385
169. Olson JS, Foley EW, Rogge C, Tsai AL, Doyle MP, Lemon DD (2004) Free Rad. Biol Med 36:685
170. Gardner PR, Gardner AM, Brashear WT, Suzuki T, Hvitved AN, Setchell KDR, Olson JS (2006) J Inorg Biochem 100:542
171. Kurtikyan TS, Ford PC (2010) Chem Commun 46:8570
172. Blomberg LM, Blomberg MRA, Siegbahn PEM (2004) J Inorg Biol Chem 9:923
173. Mishra S, Meuwly M (2010) J Am Chem Soc 132:2968
174. Møller JKS, Skibsted LH (2004) Chem Eur J 10:2291
175. Arnold EV (1996) Bohle DS 269:41
176. Munk MB, Huvaere K, Van Bocxlaer J, Skibsted LH (2010) Food Chem 121:472
177. Sarti P, Forte E, Mastronicola D, Giuffre A, Arese M (2012) Biochim Biophys Acta Bioenerget 1817:610